Hindawi
Structural Control and Health Monitoring
Volume 2023, Article ID 2076738, 21 pages
https://doi.org/10.1155/2023/2076738

Research Article

Optimal Active Vibration Control of Tensegrity Structures Using Fast Model Predictive Control Strategy

Xiaodong Feng,[1,2] **Yangbiao Fan**,[1] **Haijun Peng**,[3] **Yao Chen**,[4] **and Yiwen Zheng**[1]

[1]*School of Civil Engineering, Shaoxing University, Shaoxing 312000, China*
[2]*Department of Architecture & Architectural Engineering, Kyoto University, Kyoto 6158540, Japan*
[3]*Department of Engineering Mechanics, State Key Laboratory of Structural Analysis of Industrial Equipment, Dalian University of Technology, Dalian 116024, China*
[4]*National Prestress Engineering Research Center, Southeast University, Nanjing 211189, China*

Correspondence should be addressed to Xiaodong Feng; fengxiaodong@usx.edu.cn

Received 30 December 2022; Revised 19 May 2023; Accepted 3 August 2023; Published 7 September 2023

Academic Editor: José Rodellar

Active vibration control of tensegrity structures is often challenging due to the geometrical nonlinearity, assemblage uncertainties of connections, and actuator saturation of controllers. To tackle these technical difficulties, a fast model predictive control (FMPC) strategy is herein implemented to effectively mitigate the structural vibration. Specifically, based on the explicit expression form of the Newmark-β method, the computation of the matrix exponential is avoided and replaced by one online and two offline transient analyses at each sampling instant on the structure, and the optimal control input is attainted from the second-order dynamic equation without forming an expanded state-space equation. Meanwhile, the artificial fish swarm algorithm (AFSA) is embedded to automatically derive optimal arrangement of actuators with the selection of a reasonable objective function. Two illustrative examples, including two standard and clustered tensegrity beams and a clustered tensegrity tower, have been fully investigated. The outcomes from illustrative examples prove the effectiveness and feasibility of the proposed method in optimal active vibration control of tensegrity structures, implying a promising prospect of the investigated approach in analyzing and solving relevant engineering problems.

1. Introduction

The terminology "tensegrity" was originally coined by Fuller as a portmanteau of *tensional and integrity* [1]. Tensegrity structures are self-balanced flexible networks composed of discrete compressive rods and continuous tensile cables (Figure 1(a)). These networks form compliant, lightweight [2], and load-bearing systems [3] due to the equilibrium between compressive and tensile forces, and the structural configuration is determined by the distribution of internal forces across its components. Actually, the inclusion of rigid rods and elastic cables endows tensegrities with desirable properties such as flexibility, expandability, foldability, and movability, leading to booming applications in fields of civil and architecture [4–10], molecular mechanics and biomechanics [11–16], and aeronautics and astronautics [17–21]. Meanwhile, the concept of "tensegrity" has also been widely adopted to design functional metamaterials [22–25] and novel robots [26–30]. A fundamental feature of tensegrities is the stress bilateral property: rods and cables must be under compression and tension, respectively. In other words, cables will be slacking when bearing compressive loads, which makes the system flexible and easy to regulate with minor energy input [31, 32]. Another aspect of a tensegrity structure is that its initial structural configuration must be in stable equilibrium in absence of external forces, which to a high degree determines the structural behaviors, i.e., the stiffness to external loading. Additionally, tensegrity systems possess other potential advantages: (i) it is unnecessary to employ complex joints since compressive rods are connected to flexible cables and (ii) the structures are highly promising for active control, and therefore, the

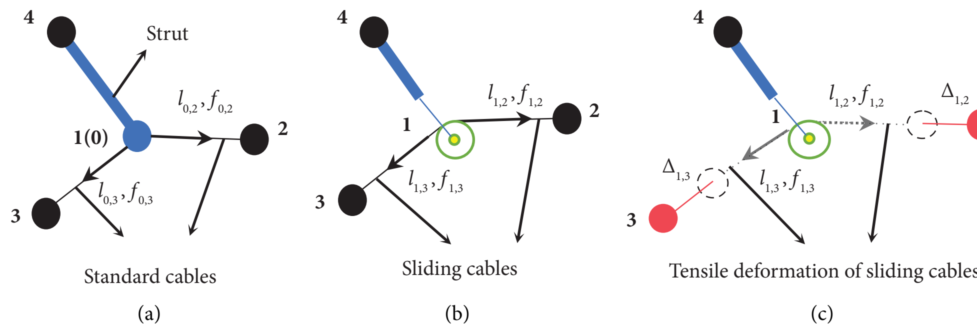

Figure 1: The connection of three members: (a) for a standard tensegrity, (b) for a clustered tensegrity, and (c) clustered cable under stretching.

systems can be easily controlled with small amount of energy [4, 33–35]. These properties create the situation that tensegrities are candidates of active and deployable structures.

For a standard tensegrity structure, pins are used to fix the joints so as to assemble the cables and struts and integrate them into a whole system, and this operation is frequently used in practical works and is necessary to simplify the construction work. By contrast, the clustered tensegrity structures are a special category of tensegrities [36], in which several individual cables are substituted by a continuous cable with the installment of several rotating pulleys to replace the corresponding pin joints. Normally, in a clustered tensegrity, cables are classified into two types, namely, the clustered and standard ones, respectively, leading to the fact that multiple solutions of initial prestress may exist to fit the static equilibrium condition of a clustered tensegrity structure that shares identical geometrical configuration with a standard one. Figures 1(b) and 1(c) depict the mechanism of a pulley connection; a clustered cable is connected by nodes 3, 1, and 2 through a rotating pulley. The pulley is assumed to be frictionless; hence, the sliding cables on both sides of pulley share the same tensile forces, while this condition does not hold in the standard cables. Hence, compared to the equivalent standard one, a clustered tensegrity will definitely possess more internal mechanisms. Accordingly, much fewer actuators are required for vibration control of clustered tensegrities, and they indeed have the potential in the regions of shape control and active actuation.

On the other hand, for the sake that tensegrities are flexible systems, the mitigation of structural dynamic responses utilizing relevant active control techniques becomes an ongoing topic in the design of real tensegrities [37–45]. Several works have been reported on numerical simulation of small and simple tensegrity models. Nevertheless, a number of demerits have been revealed for conducting different control policies, resulting in unsatisfied dynamic performance of tensegrities. Generally, there are two aspects that may cause the invalidity: (i) as a typical nonlinear system, the dynamic output of a tensegrity structure is significantly influenced by the initial equilibrium state, i.e., the prestress in components determines the global structural stiffness [46, 47]; (ii) a tensegrity structure may have several vibratory modes; thus, it is a challenge to control its dynamic behavior owing to the structural flexibility, especially in the situation of actuator saturation, namely, some structural modes may be beyond the bandwidth of a specified controller. In practical cases, the omission of actuator saturation can cause a controller designed for structures to lose stability and even fail to work [48, 49]. Fortunately, with the rapid development of computer technology, the model predictive control (MPC) has become a reality by transforming the control saturation problem into a parameter optimization problem [50–54]. The advantage of MPC is that the control saturation can be directly considered and designed in a simple manner, leading to an effective computation for physical constraints and providing satisfactory control performance. However, the application of MPC for large-scale or complicated structures requires expensive computational cost as the future structural states over the prediction horizon are predicted by utilizing the convolution integral on the first-order state equation. Inspired by this, Peng et al. developed a fast model predictive control (FMPC) method based on the standard MPC [55]; the offline computing efficiency of FMPC is several orders of magnitude higher than that of MPC without calculating matrix exponents, leading to the huge reduction of computational complexity for large structural dynamic systems. Nevertheless, to the best of the authors' knowledge, active vibration control of tensegrities via the MPC/FMPC was rarely seen.

Apart from that, in this article, the maximum and average nodal displacements are constructed as the objective function to automatically derive optimal arrangement of actuators by embedding the artificial fish swarm algorithm (AFSA). The AFSA, which is inspired by the collective movement of fish and their various social behaviors, is one of the best methods of optimization among the swarm intelligence algorithms [56]. Based on a series of instinctive behaviors, the fish always try to maintain their colonies and accordingly demonstrate intelligent behaviors. Searching for food, immigration, and dealing with dangers all happen in a social form, and interactions between all fish in a group will result in an intelligent social behavior. This algorithm has many advantages including high convergence speed, flexibility, fault tolerance, and high accuracy [57–60].

The rest of the paper is organized as follows. Section 2 describes the dynamic models of clustered and standard tensegrity structures. Section 3 introduces the formulation of the FMPC algorithm. Four types of fish behaviors, including the random, foraging, swarming, and following behaviors are discussed in Section 4. Then, in Section 5, a standard tensegrity beam, a clustered tensegrity beam, and a clustered tensegrity tower are tested in detail. Finally, Section 6 summarizes the whole process and provides further research directions.

2. Dynamic Model of Clustered and Standard Tensegrity Structures

2.1. Difference between Clustered and Standard Tensegrities. A clustered tensegrity structure normally consists of struts, standard cables, and clustered cables, in which the first two parts are the members of a standard tensegrity structure. To analyze a clustered tensegrity structure, several basic assumptions are adopted [39]:

(1) Both standard and clustered cables can only bear tensile forces.

(2) Struts and standard cables are connected by pin joints.

(3) Clustered cables are connected by frictionless pulleys.

(4) Both local buckling and global bucking of the structure are neglected.

(5) All loads are applied on joints, and the high order of stiffness increment caused by external loads is omitted.

Figure 1(a) depicts a pin-joint node that connects one strut and two standard cables of a standard tensegrity, where $l_{0,2}, l_{0,3}, l_{0,4}$ and $f_{0,2}, f_{0,3}, f_{0,4}$ denote the length and internal force of the adjacent nodes, respectively. If the aforementioned pin-joint node is substituted by a rotating pulley, as displayed in Figure 1(b), the structural configuration is then converted to the so-called clustered tensegrity structure. Equation (1) is given to illustrate the basic features of a clustered tensegrity in conformity with the mechanism properties of the pulley:

$$\begin{cases} l_{2,1,3}^{0} = l_{1,2}^{0} + l_{1,3}^{0}, \\ l_{0,4}^{0} = l_{1,4}^{0}, \\ f_{1,3}^{0} = f_{1,2}^{0}, \\ l_{2,1,3}^{t} = l_{1,2}^{t} + l_{1,3}^{t}, \\ l_{0,4}^{t} = l_{1,4}^{t}, \\ f_{1,3}^{t} = f_{1,2}^{t}, \end{cases} \tag{1}$$

where $l_{1,2}, l_{1,3}, l_{1,4}$ and $f_{1,2}, f_{1,3}, f_{1,4}$ are the member length and internal force of the corresponding members, respectively. The subscripts describe the linked nodes of cable members, and superscripts 0 and t are the initial and current structural configurations, respectively.

Normally, the pulleys balance the internal forces of the connected cables, resulting in an equilibrium state of the clustered tensegrity. Nevertheless, the occurrence of relative movements between pulleys and clustered cables leads to the unreality in controlling all nodes. More importantly, the actuation control system exerted on the clustered cables might consume less energy compared to the standard ones. This is because the structure is separated by several clusters due to the arrangement of clustered cables, and each continuous cable can be actuated by one actuator, and therefore, fewer actuators are needed in the active vibration control of clustered tensegrities. Furthermore, it is worth noting that the elemental stiffness of a clustered tensegrity is composed of two parts, namely, *Part I* that is initially originated from the standard tensegrity, and *Part II* which reveals the additional interaction stiffness of the clustered cables due to the existence of pulleys. Apparently, if the second part is eliminated from the global stiffness, the configuration of a clustered tensegrity will degenerate into a standard one [61].

2.2. Dynamic Equations for Tensegrity Structures. The dynamic equation of a tensegrity structure without control force can be expressed as

$$\mathbf{M}\ddot{\mathbf{q}}(t) + \mathbf{C}\dot{\mathbf{q}}(t) + \mathbf{K}\mathbf{q}(t) = \mathbf{L}_1\mathbf{p}(t), \tag{2}$$

where $\mathbf{M} \in \mathbb{R}^{n\times n}$, $\mathbf{C} \in \mathbb{R}^{n\times n}$, and $\mathbf{K} \in \mathbb{R}^{n\times n}$ refer to the global mass, damping matrix, and stiffness matrix, respectively. $\mathbf{q} \in \mathbb{R}^{n\times 1}$, $\dot{\mathbf{q}} \in \mathbb{R}^{n\times 1}$, and $\ddot{\mathbf{q}} \in \mathbb{R}^{n\times 1}$ represent the vector of nodal displacement, velocity, and acceleration, respectively. $\mathbf{L}_1 \in \mathbb{R}^{n\times \overline{m}}$ and $\mathbf{p} \in \mathbb{R}^{\overline{m}\times 1}$ are the position matrix of external forces and the vector of external forces, respectively.

The global mass and stiffness matrix can be formulated by the following equation [39]:

$$\begin{cases} \mathbf{M} = \sum\left(\Pi\mathbf{M}_e\Pi^T\right), \\ \mathbf{K} = \sum\left(\Pi\mathbf{K}_e\Pi^T\right), \end{cases} \tag{3}$$

where $\mathbf{M}_e \in \mathbb{R}^{6\times 6}$ and $\mathbf{K}_e \in \mathbb{R}^{6\times 6}$ are the elemental mass and stiffness matrix, respectively. Π is the connectivity matrix that can be derived from classical finite element method. Table 1 gives the details of constructing structural stiffness matrices of clustered tensegrities.

If a control system is applied onto the structure, the dynamic equations can be written as

$$\mathbf{M}\ddot{\mathbf{q}}(t) + \mathbf{C}\dot{\mathbf{q}}(t) + \mathbf{K}\mathbf{q}(t) = \mathbf{L_1}\mathbf{p}(t) + \mathbf{L_2}\mathbf{u}(t), \tag{4}$$

where $\mathbf{L_2} \in \mathbb{R}^{n\times m}$ is the position matrix of control inputs and $\mathbf{u} \in \mathbb{R}^{m\times 1}$ is the vector of control forces.

In order to achieve a state-space representation of the controlled system, it usually converts the dynamic equation into a state-space formulation, which yields

Table 1: The procedure of constructing stiffness matrices of clustered tensegrity structures.

Step	Parameters	Remarks	
	$[x_i^0, y_i^0, z_i^0]\,[x_j^0, y_j^0, z_j^0]$	Nodal coordinates at t_0	
	$[x_i^t, y_i^t, z_i^t]\,[x_j^t, y_j^t, z_j^t]$	Nodal coordinates at t	
1	$\mathbf{q} = [q_1, \cdots, q_{n_e}, \cdots, q_n]$	Elemental preloading vector	Global operation
	E	Young's modulus	
	A_c	Elemental cross-sectional area	
	$\Delta_{2,1,3} = l_{2,1,3}^t - l_{2,1,3}^0$	Displacement of nodes 2, 1, 3	
2	$\Delta_{2,1,3} = \Delta_{1,2} + \Delta_{1,3}$		
	where $\Delta_{1,2} = l_{1,2}^t - l_{1,2}^0$	Displacement of nodes 1, 2	
	$\Delta_{1,3} = l_{1,3}^t - l_{1,3}^0$	Displacement of nodes 1, 3	
	$\varepsilon_0 = q_{n_e}/EA_c$	Elemental initial strain	
3	$\varepsilon = \Delta_{2,1,3}/l_{2,1,3}^0 + \varepsilon_0$	Strain at time t	
	$\sigma = EA_c\varepsilon$	Stress at time t	
	$\mathbf{K}_1^t = \sum_{i=1}^2 \mathbf{K}_1^i + \sum_{i=1}^2 \overline{\mathbf{K}}_1^i$		
	$\mathbf{K}_1^i = \mathbf{T}_i^T \mathbf{K}_e \mathbf{T}_i$	$i = [1, 2]$	
	$\overline{\mathbf{K}}_1^i = \mathbf{T}_i^T \mathbf{K}_e \mathbf{T}_j$	$j = [1, 2]; i \neq j$	
	where $\mathbf{K}_e = EA_c/l_{2,1,3}^0 \mathbf{c}_l \mathbf{c}_l^T$		
	$\mathbf{c}_l = [-1, 1]^T$		
4	$\mathbf{T}_i = \begin{bmatrix} c_1^i & c_2^i & c_3^i & 0 & 0 & 0 \\ 0 & 0 & 0 & c_1^i & c_2^i & c_3^i \end{bmatrix}$		Local operation
	$c_1^i = \cos(\alpha_i) = x_m^0 - x_n^0 + u_m - u_n/l_{m,n}^t$	$m = 1; n = [3, 2]$	
	$c_2^i = \cos(\beta_i) = y_m^0 - y_n^0 + v_m - v_n/l_{m,n}^t$		
	$c_3^i = \cos(\gamma_i) = z_m^0 - z_n^0 + w_m - w_n/l_{m,n}^t$		
	$u_m = x_m^t - x_m^0; u_n = x_n^t - x_n^0$		
	$v_m = y_m^t - y_m^0; v_n = y_n^t - y_n^0$		
	$w_m = z_m^t - z_m^0; w_n = z_n^t - z_n^0$		
	$\mathbf{d}_g = [u_m, v_m, w_m, u_n, v_n, w_n]$		
	$\mathbf{K}_2^t = \sum_{i=1}^2 \mathbf{K}_2^i$		
	$\mathbf{K}_2^i = A_c\sigma/l_{m,n}^t [\mathbf{Y}_c 1/l_{m,n}^t \mathbf{J}_i \mathbf{J}_i^T]$		
5	$\mathbf{Y}_c = \mathbf{Y}_y \mathbf{Y}_y^T$		
	$\mathbf{Y} = [-\mathbf{I}_{3\times 3} \mathbf{I}_{3\times 3}]^T$		
	$\mathbf{J}_i = l_{m.n}^t [-c_1^i, c_1^i, -c_2^i, c_2^i, -c_3^i, c_3^i]$		
6	$\mathbf{K}_{b_e} = \mathbf{K}_1^t + \mathbf{K}_2^t$		
7	$\mathbf{K}_b = \sum(\Pi \mathbf{K}_{b_e} \Pi^T)$ Π: standard FEM connectivity	Global stiffness matrix	Global operation

$$\dot{\mathbf{x}}(t) = \mathbf{A}\mathbf{x}(t) + \mathbf{B}\mathbf{u}(t) + \mathbf{G}\mathbf{p}(t), \tag{5}$$

$$\begin{aligned} \mathbf{x} &= \begin{Bmatrix} \mathbf{q} \\ \dot{\mathbf{q}} \end{Bmatrix}, \\ \mathbf{A} &= \begin{bmatrix} \mathbf{0}_n & \mathbf{I}_n \\ -\mathbf{M}^{-1}\mathbf{K} & -\mathbf{M}^{-1}\mathbf{C} \end{bmatrix}, \\ \mathbf{B} &= \begin{bmatrix} \mathbf{0}_n \\ \mathbf{M}^{-1}\mathbf{L}_2 \end{bmatrix}, \\ \mathbf{G} &= \begin{bmatrix} \mathbf{0} \\ \mathbf{M}^{-1}\mathbf{L}_1 \end{bmatrix}, \end{aligned} \tag{6}$$

where $\mathbf{x}$ is the state vector, $\mathbf{A}$, $\mathbf{B}$, $\mathbf{G}$, $\mathbf{0}_n$, and $\mathbf{I}_n$ are the state matrix, input matrix, environmental disturbance position matrix, zero matrix, and unit matrix, respectively.

The output vector is written as follows:

$$\mathbf{y} = \overline{\mathbf{S}}\mathbf{x}, \tag{7}$$

where $\mathbf{y} \in \mathbb{R}^{\xi\times 1}$ is the output vector, $\overline{\mathbf{S}} \in \mathbb{R}^{\xi\times 2n}$ is the output matrix, and ξ is the number of output variables.

3. Formulation of the FMPC Algorithm

3.1. Explicit Expression Form of the Newmark-β Method. In the standard MPC, the future states of the structural responses are predicted by employing the convolution integral; however, they are predicted by utilizing the explicit expression form of the Newmark-β method in the FMPC algorithm.

The dynamic equation omitting external forces from equation (4) can be rewritten as

$$\mathbf{M}\ddot{\mathbf{q}}(t) + \mathbf{C}\dot{\mathbf{q}}(t) + \mathbf{K}\mathbf{q}(t) = \mathbf{L}_2\mathbf{u}(t). \tag{8}$$

In the Newmark-β method, concerning the velocity and displacement, the relationship between the adjacent time steps is as follows:

$$\dot{\mathbf{q}}_{k+1} = \dot{\mathbf{q}}_k + [(1-\delta)\ddot{\mathbf{q}}_k + \delta\ddot{\mathbf{q}}_{k+1}]\Delta t, \tag{9}$$

$$\mathbf{q}_{k+1} = \mathbf{q}_k + \dot{\mathbf{q}}_k\Delta t + \left[\left(\frac{1}{2}-\alpha\right)\ddot{\mathbf{q}}_k + \alpha\ddot{\mathbf{q}}_{k+1}\right](\Delta t)^2, \tag{10}$$

where Δt is the length of time step and parameters α and $\delta\,(\delta \geq 0.5, \alpha \geq 0.25\,(0.5+\delta)^2)$ are the coefficients that determine the stability and accuracy of the algorithm. At time step $t_{k+1} = t_k + \Delta t$, the dynamic responses (displacement, velocity, and acceleration) must satisfy the dynamic equilibrium condition, given by

$$\mathbf{M}\ddot{\mathbf{q}}_{k+1} + \mathbf{C}\dot{\mathbf{q}}_{k+1} + \mathbf{K}\mathbf{q}_{k+1} = \mathbf{L}_2\mathbf{u}_{k+1}. \tag{11}$$

The dynamic responses at time step t_{k+1} can be obtained by combining equations (9) and (10), given as

$$\mathbf{q}_{k+1} = \hat{\mathbf{K}}^{-1}\mathbf{L}_2\mathbf{u}_{k+1} + \Theta_{11}\mathbf{q}_k + \Theta_{12}\dot{\mathbf{q}}_k + \Theta_{13}\ddot{\mathbf{q}}_k, \tag{12}$$

$$\dot{\mathbf{q}}_{k+1} = b_1\hat{\mathbf{K}}^{-1}\mathbf{L}_2\mathbf{u}_{k+1} + \Theta_{21}\mathbf{q}_k + \Theta_{22}\dot{\mathbf{q}}_k + \Theta_{23}\ddot{\mathbf{q}}_k, \tag{13}$$

$$\ddot{\mathbf{q}}_{k+1} = b_4\hat{\mathbf{K}}^{-1}\mathbf{L}_2\mathbf{u}_{k+1} + \Theta_{31}\mathbf{q}_k + \Theta_{32}\dot{\mathbf{q}}_k + \Theta_{33}\ddot{\mathbf{q}}_k, \tag{14}$$

where $\hat{\mathbf{K}}$ is the equivalent stiffness matrix.

$$\hat{\mathbf{K}} = b_4\mathbf{M} + b_1\mathbf{C} + \mathbf{K}. \tag{15}$$

The detailed expressions of coefficients $\Theta_{\mu\nu}\,(\mu, \nu = 1,2,3)$ and $b_\varsigma\,(\varsigma = 1,2,3,4,5,6)$ in calculating equations (12)–(15) can be found in Appendix.

Normally, the dynamic response at time steps t_k and t_{k+1} can be expressed as

$$\mathbf{v}_k = \begin{Bmatrix} \mathbf{q}_k \\ \dot{\mathbf{q}}_k \\ \ddot{\mathbf{q}}_k \end{Bmatrix}, \quad \mathbf{v}_{k+1} = \begin{Bmatrix} \mathbf{q}_{k+1} \\ \dot{\mathbf{q}}_{k+1} \\ \ddot{\mathbf{q}}_{k+1} \end{Bmatrix}. \tag{16}$$

Hence, substitute equations (12)–(14) into (16), which yields

$$\mathbf{v}_{k+1} = \mathbf{h}\mathbf{v}_k + \mathbf{w}\mathbf{u}_{k+1}, \tag{17}$$

where

$$\mathbf{h} = \begin{bmatrix} \Theta_{11} & \Theta_{12} & \Theta_{13} \\ \Theta_{21} & \Theta_{22} & \Theta_{23} \\ \Theta_{31} & \Theta_{32} & \Theta_{33} \end{bmatrix}, \quad \mathbf{w} = \begin{bmatrix} \hat{\mathbf{K}}^{-1}\mathbf{L}_2 \\ b_1\hat{\mathbf{K}}^{-1}\mathbf{L}_2 \\ b_4\hat{\mathbf{K}}^{-1}\mathbf{L}_2 \end{bmatrix}. \tag{18}$$

The initial dynamic response $\mathbf{v}_0 = [\mathbf{q}_0^T, \dot{\mathbf{q}}_0^T, \ddot{\mathbf{q}}_0^T]^T$ can be obtained by substituting the initial state $\mathbf{x}_0 = [\mathbf{q}_0^T, \dot{\mathbf{q}}_0^T]^T$ into Equation (11). at time step t_0, which yields

$$\mathbf{v}_0 = \mathbf{f}_1\mathbf{x}_0 + \mathbf{f}_2\mathbf{u}_0, \tag{19}$$

where

$$\mathbf{f}_1 = \begin{bmatrix} \mathbf{I}_n & \mathbf{0} \\ \mathbf{0} & \mathbf{I}_n \\ -\mathbf{M}^{-1}\mathbf{K} & -\mathbf{M}^{-1}\mathbf{C} \end{bmatrix}, \quad \mathbf{f}_2 = \begin{bmatrix} \mathbf{0} \\ \mathbf{0} \\ \mathbf{M}^{-1}\mathbf{L}_2 \end{bmatrix}. \tag{20}$$

By performing an iterative computation of (17), the future dynamic responses for all time steps can be described as

$$\mathbf{v}_k = \hat{\mathbf{H}}_k\mathbf{x}_0 + \sum_{j=0}^{k}\hat{\mathbf{W}}_{k,j}\mathbf{u}_j, \quad 1 \leq k \leq N, \tag{21}$$

where N is the total number of time steps.

$$\hat{\mathbf{H}}_k = \mathbf{h}^k\mathbf{f}_1, \quad \hat{\mathbf{W}}_{k,j} = \begin{cases} \mathbf{h}^k\mathbf{f}_2, & j = 0, \\ \mathbf{h}^{k-j}\mathbf{w}, & 1 \leq j \leq k. \end{cases} \tag{22}$$

Equation (21) can be rewritten in matrix form as follows:

$$\mathbf{V} = \hat{\mathbf{H}}\mathbf{x}_0 + \hat{\mathbf{W}}\mathbf{u} = \begin{bmatrix} \mathbf{h}\mathbf{f}_1 \\ \mathbf{h}^2\mathbf{f}_1 \\ \mathbf{h}^3\mathbf{f}_1 \\ \vdots \\ \mathbf{h}^N\mathbf{f}_1 \end{bmatrix}\mathbf{X}_0 + \begin{bmatrix} \mathbf{h}\mathbf{f}_2 & \mathbf{w} & \mathbf{0} & \cdots & \mathbf{0} \\ \mathbf{h}^2\mathbf{f}_2 & \mathbf{h}\mathbf{w} & \mathbf{w} & \cdots & \mathbf{0} \\ \mathbf{h}^3\mathbf{f}_2 & \mathbf{h}^2\mathbf{w} & \mathbf{h}\mathbf{w} & \cdots & \mathbf{0} \\ \vdots & \vdots & \vdots & \ddots & \vdots \\ \mathbf{h}^N\mathbf{f}_2 & \mathbf{h}^{N-1}\mathbf{w} & \mathbf{h}^{N-2}\mathbf{w} & \cdots & \mathbf{w} \end{bmatrix}\begin{Bmatrix} \mathbf{u}_0 \\ \mathbf{u}_1 \\ \mathbf{u}_2 \\ \vdots \\ \mathbf{u}_N \end{Bmatrix}, \tag{23}$$

where $\mathbf{V}$ is the aggregation of all future dynamic responses.

According to explicit expression form in (21) and the output (7), the future outputs $\mathbf{y}_k$ for all prediction points are given as follows:

$$\mathbf{y}_k = \hat{\mathbf{S}}\hat{\mathbf{H}}_k\mathbf{x}_0 + \sum_{j=0}^{k}\hat{\mathbf{S}}\mathbf{W}_{k,j}\mathbf{u}_j, \quad 1 \le k \le N, \tag{24}$$

where $\hat{\mathbf{S}} = \begin{bmatrix} \overline{\mathbf{S}} & \mathbf{0} \end{bmatrix}$ is a $\xi \times 3n$ matrix.

Equation (24) can also be expressed in matrix form:

$$\mathbf{Y} = \mathbf{F}\mathbf{x}_0 + \mathbf{G}\mathbf{U} = \hat{\mathbf{S}}.*\mathbf{H}\mathbf{x}_0 + \hat{\mathbf{S}}.*\mathbf{W}\mathbf{U}. \tag{25}$$

The symbol $.*$ denotes that if A is a $m \times p$ dimensional matrix and B is a $k \times l$ block matrix with $p \times n$ dimensional submatrices, then $\mathbf{A}.*\mathbf{B}$ is a $k \times l$ block matrix with $m \times n$ dimensional submatrices:

$$\mathbf{A}.*\mathrm{B} = \begin{bmatrix} \mathbf{AB}_{11} & \cdots & \mathbf{AB}_{1l} \\ \vdots & \ddots & \vdots \\ \mathbf{AB}_{k1} & \cdots & \mathbf{AB}_{kl} \end{bmatrix}. \tag{26}$$

Hence, the performance index $\mathbf{J}$ is given as

$$\mathbf{J} = \frac{1}{2}\mathbf{Y}^T\mathbf{Q}\mathbf{Y} + \frac{1}{2}\mathbf{U}^T\mathbf{R}\mathbf{U}, \tag{27}$$

where $\mathbf{Q} \in \mathbb{R}^{N\xi\times N\xi}$ isa nonnegative definite symmetric weighting matrix and $\mathbf{R} \in \mathbb{R}^{Nm\times Nm}$ is a positive definite symmetric weighting matrix.

The optimal control input sequence $\mathbf{U}$ is subsequently achieved by minimizing the performance index $\mathbf{J}$ given in equation (27), which yields

$$\begin{aligned} \mathbf{U} &= -\left(\mathbf{G}^T\mathbf{Q}\mathbf{G} + \mathbf{R}\right)^{-1}\mathbf{G}^T\mathbf{Q}\mathbf{F}x_0 \\ &= -\overline{\mathbf{K}}\mathbf{x}_0. \end{aligned} \tag{28}$$

3.2. Fast Computation for FMPC. The optimal control input sequence $\mathbf{U}$ can be divided into two parts, namely, the offline part $\overline{\mathbf{K}}_1$ and the online part $\overline{\mathbf{K}}_2$:

$$\mathbf{U} = -\overline{\mathbf{K}}_1\overline{\mathbf{K}}_2, \tag{29}$$

where

$$\overline{\mathbf{K}}_1 = \left(\left(\hat{\mathbf{S}}.*\hat{\mathbf{W}}\right)^T\mathbf{Q}\left(\hat{\mathbf{S}}.*\hat{\mathbf{W}}\right) + \mathbf{R}\right)^{-1}\left(\hat{\mathbf{S}}.*\hat{\mathbf{W}}\right)^T\mathbf{Q}, \tag{30}$$

$$\overline{\mathbf{K}}_2 = \hat{\mathbf{S}}.*\hat{\mathbf{H}}\mathbf{x}_0. \tag{31}$$

According to the above equations, the key for computation of $\overline{\mathbf{K}}_1$ and $\overline{\mathbf{K}}_2$ is to obtain matrix $\mathbf{W}$ and $\mathbf{H}\mathbf{x}_0$, respectively. Therefore, the fast computations of these two matrices are taken into account.

3.2.1. Fast Computation for Matrix $\hat{\mathbf{W}}$. As is observed from equation (23), as the other block columns can be easily computed from $\hat{\mathbf{W}}_{k,2}$, only the first two block columns ($\hat{\mathbf{W}}_{k,1}$ and $\hat{\mathbf{W}}_{k,2}$) in matrix $\mathbf{W}$ need to be determined. According to the physical meaning of matrix $\hat{\mathbf{W}}_{k,j}$, $\hat{\mathbf{W}}_{k,1}$ and $\hat{\mathbf{W}}_{k,2}$ can be derived by setting the initial state $\mathbf{x}_0 = \mathbf{0}$ and applying the unit control input $\mathbf{u}_0 = \mathbf{I}_m$ onto the dynamic system at time steps t_0 and t_1, respectively. Therefore, the dynamic responses for all time steps can be formulated into following forms:

$$\begin{aligned} \mathbf{V} &= \begin{bmatrix} \mathbf{hf}_2 & \mathbf{w} & \mathbf{0} & \cdots & \mathbf{0} \\ \mathbf{h}^2\mathbf{f}_2 & \mathbf{hw} & \mathbf{w} & \cdots & \mathbf{0} \\ \mathbf{h}^3\mathbf{f}_2 & \mathbf{h}^2\mathbf{w} & \mathbf{hw} & \cdots & \mathbf{0} \\ \vdots & \vdots & \vdots & \ddots & \vdots \\ \mathbf{h}^N\mathbf{f}_2 & \mathbf{h}^{N-1}\mathbf{w} & \mathbf{h}^{N-2}\mathbf{w} & \cdots & \mathbf{w} \end{bmatrix} \begin{Bmatrix} \mathbf{I}_m \\ \mathbf{0} \\ \mathbf{0} \\ \vdots \\ \mathbf{0} \end{Bmatrix} \\ &= \begin{bmatrix} \mathbf{hf}_2 \\ \mathbf{h}^2\mathbf{f}_2 \\ \mathbf{h}^3\mathbf{f}_2 \\ \vdots \\ \mathbf{h}^N\mathbf{f}_2 \end{bmatrix} \\ &= \hat{\mathbf{W}}_{k,1}, \end{aligned} \tag{32}$$

$$\begin{aligned} \mathbf{V} &= \begin{bmatrix} \mathbf{hf}_2 & \mathbf{w} & \mathbf{0} & \cdots & \mathbf{0} \\ \mathbf{h}^2\mathbf{f}_2 & \mathbf{hw} & \mathbf{w} & \cdots & \mathbf{0} \\ \mathbf{h}^3\mathbf{f}_2 & \mathbf{h}^2\mathbf{w} & \mathbf{hw} & \cdots & \mathbf{0} \\ \vdots & \vdots & \vdots & \ddots & \vdots \\ \mathbf{h}^N\mathbf{f}_2 & \mathbf{h}^{N-1}\mathbf{w} & \mathbf{h}^{N-2}\mathbf{w} & \cdots & \mathbf{w} \end{bmatrix} \begin{Bmatrix} \mathbf{0} \\ \mathbf{I}_m \\ \mathbf{0} \\ \vdots \\ \mathbf{0} \end{Bmatrix} \\ &= \begin{bmatrix} \mathbf{w} \\ \mathbf{hw} \\ \mathbf{h}^2\mathbf{w} \\ \vdots \\ \mathbf{h}^{N-1}\mathbf{w} \end{bmatrix} \\ &= \hat{\mathbf{W}}_{k,2}. \end{aligned} \tag{33}$$

Equations (32) and (33) denote that $\hat{\mathbf{W}}_{k,1}$ and $\hat{\mathbf{W}}_{k,2}$ can be obtained by carrying out one transient analysis on the dynamic system using the Newmark-β method with a zero initial state and a unit control input at time steps t_0 and t_1.

3.2.2. Fast Computation for Matrix $\hat{\mathbf{H}}\mathbf{x}_0$. According to the explicit expression form of the Newmark-β method, if only an initial state $\mathbf{x}_0$ is applied to the system (without control input), the dynamic responses for all time steps can be rewritten as

$$\mathbf{V} = \hat{\mathbf{H}}\mathbf{x}_0. \tag{34}$$

Equation (34) shows that $\hat{\mathbf{H}}\mathbf{x}_0$ can be computed by carrying out one transient analysis on the dynamic system with the setting of initial state $\mathbf{x}_0$ without control input.

Once $\overline{\mathbf{K}}_1$ and $\overline{\mathbf{K}}_2$ are determined, the optimal control input $\mathbf{U}$ can be attainted according to (29).

4. The Artificial Fish Swarm Algorithm (AFSA)

The AFSA, which was developed by Li et al. [62], is a population-based optimization technique inspired by natural fish swarm schooling behaviors. Due to the efficiency in solving engineering issues, AFSA has gained vast popularity in the past few decades. As a typical swarm intelligent algorithm, each artificial fish hunts for food in conformity with its own manner, including but not limited to random, foraging, swarming, and following behaviors. Each artificial fish allows mutual information communications until attaining a global optimum. More importantly, the gradient information is not a necessary condition in the process of the optimization. Hence, AFSA is widely adopted in the searching of global optimal solutions due to the fact that it takes full advantage of the concentrated emerging mechanism of the individual intelligence [63].

The concept of AFSA is described as follows: a fish swarm comprised of N artificial fish exists in a d-dimensional space. Let $\mathbf{T}_i = (T_{i1}, T_{i2}, \cdots, T_{iD})$ denote the current position of an artificial fish, namely, the position matrix of control inputs $\mathbf{L}_2$ in equation (4); the food consistency (the objective function) that this designated fish at position T_i can recognize is depicted as $O_i = f(T_i)$. *Visual*, δ, and *Step*, respectively, reflect the perceiving range, the congestion factor, and the moving step. Detailed definitions of the four behaviors are as follows.

4.1. Random Behavior. This is a default behavior, which describes a phenomenon that in the *visual* range of a fish, the fish randomly selects a target position and moves towards it.

4.2. Foraging Behavior. Foraging is known as the basic behavior to search for food, which is on the basis of a random forage with a tendency towards food concentration. Let T_j represent the position in the visual range of a fish at the current time. For a mathematical minimization problem, if $O_j < O_i$, the fish will move a *Step* forward in the direction of $(T_j - T_i)$. If not, randomly select a new state T_j and judge whether it can meet the forward condition. The random behavior is performed if the foraging behavior is invalid after preset try-number times, and therefore, the position T_i^* can be updated as

$$T_i^* = \begin{cases} T_i + \dfrac{T_j - T_i}{d_{\mathrm{ij}}} \bullet step \bullet \mathrm{rand}, & \text{if } O_j < O_\mathrm{i}, \\ \text{random behavior}, & \text{otherwise}, \end{cases} \tag{35}$$

where $d_{\mathrm{ij}} = \|T_i - T_j\|$ denotes the distance between T_i and T_j and rand is generated uniformly within the range [0, 1].

4.3. Swarming Behavior. Fish are species that are sensitive to the external environment, and they usually gather in several groups to minimize possible threats. In a fish swarm of N_F artificial fish, the central position T_c is explored by each fish T_i in its current neighborhood ($d_{\mathrm{ij}} < Visual$). Meanwhile, fish T_i will step forward to T_c if it satisfies the condition $O_c/N_F < \delta \cdot O_i$.

Theoretically,

$$T_i^* = \begin{cases} T_i + \dfrac{T_c - T_i}{d_{ic}} \bullet \mathrm{step} \bullet \mathrm{rand}, & \text{if } \dfrac{O_c}{N_F} < \delta \cdot O_i, \\ \text{foraging behavior}, & \text{otherwise}, \end{cases} \tag{36}$$

where δ represents the food concentration factor between 0 and 1.

4.4. Following Behavior. If one fish is located in a position with a large food concentration coefficient, other fish will follow their neighbors to feed within their visual range. Suppose $T_{\mathrm{best}(l)}$ is the local best companion in the current neighborhood of T_i. If $O_{\mathrm{best}(l)}/N_F < \delta \cdot O_i$, fish T_i then attempts to step forward in the direction $(T_{\mathrm{best}(l)} - T_i)$. The following behavior can be conducted as

$$T_i^* = \begin{cases} T_i + \dfrac{T_{\mathrm{best}(l)} - T_i}{d_{i,\mathrm{best}(l)}} \bullet \mathrm{step} \bullet \mathrm{rand}, & \text{if } \dfrac{O_{\mathrm{best}(l)}}{N_F} < \delta \cdot O_i, \\ \text{foraging behavior}, & \text{otherwise}. \end{cases} \tag{37}$$

The aforementioned four behaviors are compared and implemented for each artificial fish. Nonetheless, only the best behavior is chosen to renew the current position. Additionally, in a fish swarm, bulletin is employed to record the optimum state O_{best}. In other words, in each step, the state of each fish is compared with the former one, and better state will be renewed automatically in the bulletin.

Overall, Figure 2 gives the flowchart of achieving optimal control strategy using the proposed method. The proposed control strategy can be decomposed into two segments, namely, the FMPC and the AFSA. The FMPC algorithm works online since the control input sequence $\mathbf{U}$ is determined by the structural state at each time. Strictly, AFSA is an offline swarm intelligence algorithm, and the function of conducting the AFSA algorithm in this article is only to acquire the optimal actuator placement. However, it is worth mentioning that during the optimization of AFSA, the reservation of elite fish relies on the comparison of output information (the current structural state determined by the control input sequence $\mathbf{U}$) generated from FMPC, and therefore, AFSA also works online in this sense.

5. Numerical Case Study

In this section, three illustrative examples including a standard tensegrity beam, a clustered tensegrity beam, and a clustered tensegrity tower are studied utilizing MATLAB (R2021b) platform. The results imply that the presented methods work remarkably well on active vibration control for both standard and clustered tensegrity structures, and reasonable control effect is achieved with optimal arrangement of actuators. In control design, the self-weight of the structure was ignored, i.e., the gravity was not considered, and the weighting matrices are chosen as $\mathbf{Q} = 1 \times 10^7 \mathbf{I}_1$

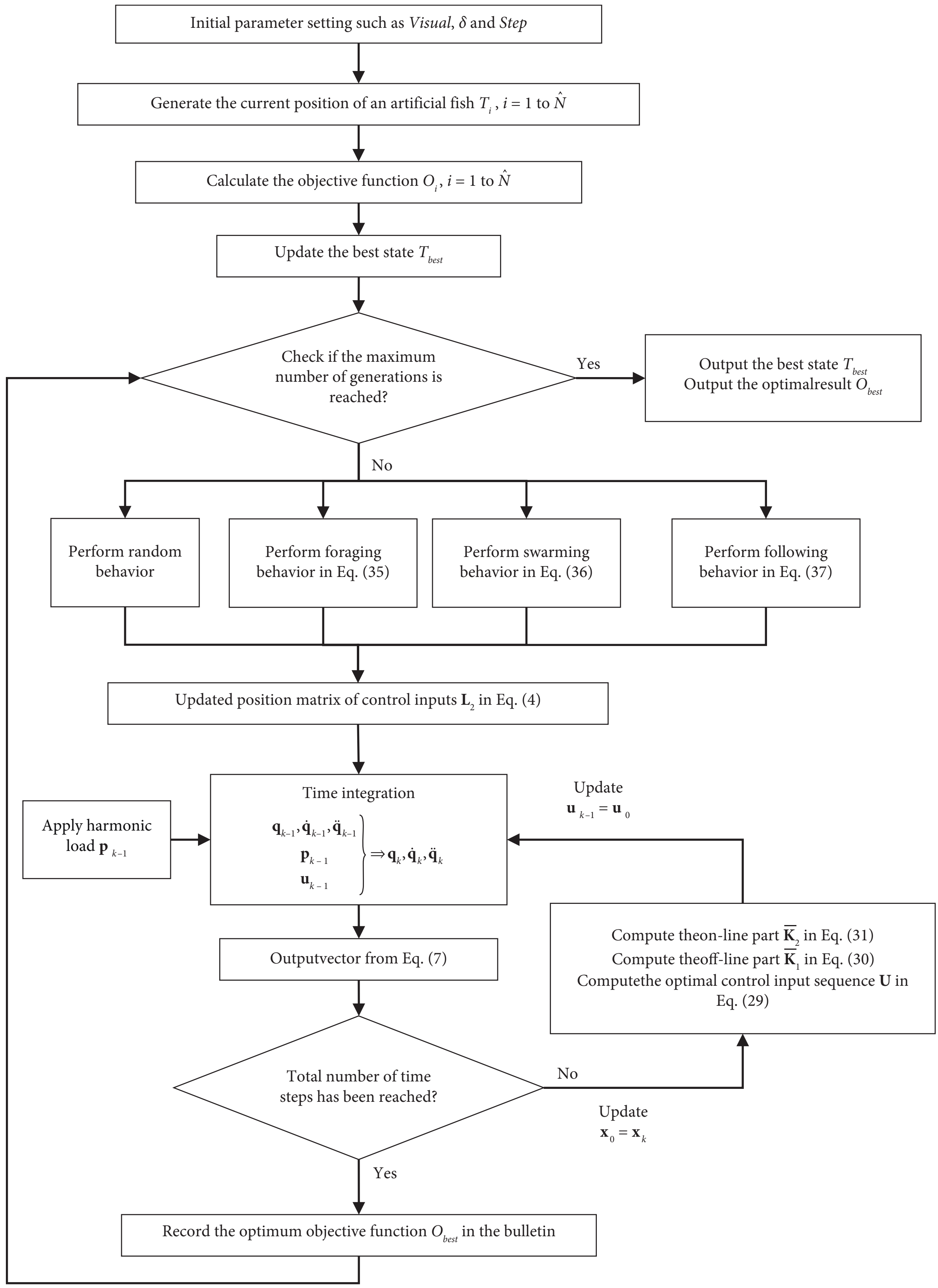

Figure 2: The flowchart of achieving optimal control strategy using the proposed method.

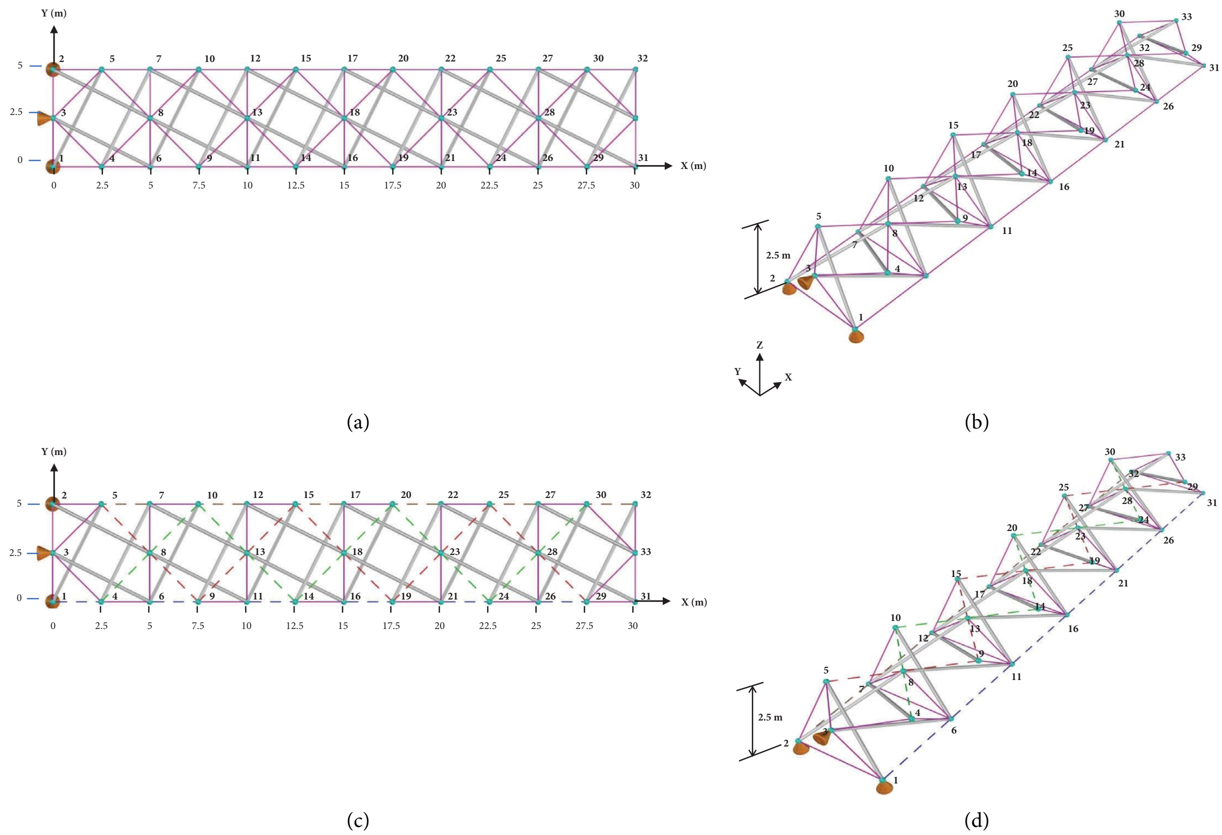

Figure 3: The spatial double-layer standard tensegrity beam and clustered tensegrity beam formed by 6 quadruplex units: (a) top view, (b) perspective view, (c) top view, and (d) perspective view.

and $\mathbf{R} = 1 \times 10^{-2}\mathbf{I}_2$, where $\mathbf{I}_1 \in \mathbb{R}^{N\zeta \times N\zeta}$ and $\mathbf{I}_2 \in \mathbb{R}^{Nm \times Nm}$ are unit matrices.

5.1. Standard and Clustered Tensegrity Cantilever Beams. Two numerical models with identical topological connectivity and geometrical configuration for standard and clustered tensegrity beams, as shown in Figure 3, are herein adopted for comparison purpose. Each structure is composed of 6 quadruple units with 24 struts and 67 cables, among which 32 clustered cables for clustered tensegrity beam are denoted by dashed lines in four colors, and line in the same color represents a clustered cable with identical attribute. For example, the green and brown dashed lines that respectively connects nodes 4, 8, 10, 13, 14, 18, 20, 23, 24, 28, and 30 and nodes 1, 6, 11, 16, 21, 26, and 31 are upper and lower clustered cables. The purple and grey solid lines represent the corresponding struts and standard cables, respectively. Besides, nodes 1, 2, and 3 were completely fixed as the boundary condition to simulate a cantilever beam. Tables 2 and 3 give the geometrical and mechanical parameters of elements, which were determined from our previous studies [64–66].

A harmonic function $\mathbf{P}(\mathrm{t})$, which was applied in the Z-direction on each node with time step of 0.020 s, was selected as the external loading (N), given as

$$\mathbf{P}(t) = 10000\sin(2t + 40), \quad t \in [0 \quad 30]. \tag{38}$$

To be clear, the control rate in this article is defined as the ratio of nodal displacement difference (generated by uncontrolled and controlled status) to the uncontrolled nodal displacement. Figure 4 shows the displacement curves of nodes 10, 12, 15, 17, 20, 25, 30, and 32 in the Z-direction for standard and clustered tensegrity cantilever beams with four actuators located at nodes 28, 31, 32, and 33. Table 4 displays the comparative results on maximum displacement and the corresponding control efficiency in mitigating nodal displacement. For the standard tensegrity cantilever beam, the maximum displacement of node 17 situated at midspan was 1.72 m without control, and it diminished to 0.75 m with the intervention of FMPC control (with a reduction rate of 56.26%). More interestingly, with the aid of actuators installed at the end of the cantilever beam, the maximum displacement of the ending node 32 acquired a sharp decline form 2.13 m to 0.71 m after control (with a reduction rate of 66.50%), even smaller than that of node 17. Similar phenomena can be found in the cases of the clustered tensegrity beam, indicating the effectiveness of the FMPC method in active vibration control of both standard and clustered tensegrity structures. Additionally, for a same control policy, i.e., the identical number and placement of actuators, the clustered tensegrity beam vibrates faster to a stable state compared to

Table 2: Geometrical and mechanical properties of standard and clustered tensegrity beams.

Parameter	Standard tensegrity structure	Clustered tensegrity structure
Cross section of struts	$3.2 \times 10^{-2} m^2$	$3.2 \times 10^{-2} m^2$
Cross section of cables	$1 \times 10^{-3} m^2$	$1 \times 10^{-3} m^2$
Young's modulus of struts	$200 \times 10^9 Pa$	$200 \times 10^9 Pa$
Young's modulus of cables	$40 \times 10^9 Pa$	$40 \times 10^9 Pa$
Density of cables and struts	$7800\,kg/m^3$	$7800\,kg/m^3$
Prestress in struts	Refer to Table 3	−385000 N
Prestress in peripheral lower cables		192500 N
Prestress in internal lower cables		192500 N
Prestress in upper cables		385000 N
Prestress in bracing cables		385000 N

Table 3: Prestress for standard tensegrity structure beam.

Upper cables			Lower cables			Bracing cables			Struts		
Node number		Prestress (N)	Node number		Prestress (N)	Node number		Prestress (N)	Node number		Prestress (N)
4	8	357360.98	1	2	178680.49	2	5	357360.98	1	5	−357360.98
8	10	226459.55	6	7	291910.27	7	8	341701.51	4	7	−357360.98
10	13	226459.55	11	12	320102.26	4	6	357360.98	2	8	−357360.98
13	14	310531.21	16	17	316279.94	1	3	357360.98	3	6	−357360.98
14	18	310531.21	21	22	325044.97	7	10	226459.55	8	11	−210800.08
18	20	322028.67	26	27	307049.18	12	13	127874.25	6	10	−226459.55
20	23	322028.67	31	32	172240.35	9	11	195140.61	9	12	−195140.61
23	24	269617.66	1	6	178680.49	6	8	226459.55	7	13	−210800.08
24	28	269617.66	6	11	113229.78	12	15	445063.92	13	16	−377797.56
28	30	344480.70	11	16	222531.96	17	18	311521.65	12	18	−377797.56
5	8	357360.98	16	21	161014.33	14	16	310531.21	11	15	−445063.92
8	9	195140.61	21	26	163040.19	11	13	460723.39	14	17	−310531.21
9	13	195140.61	26	31	172240.35	17	20	322028.67	18	21	−323019.11
13	15	445063.92	2	7	178680.49	22	23	295778.19	17	23	−323019.11
15	18	445063.92	7	12	97570.30	19	21	324009.55	16	20	−322028.67
18	19	324009.55	12	17	155265.60	16	18	389295.02	19	22	−324009.55
19	23	324009.55	17	22	162004.78	22	25	326080.39	23	26	−297849.03
23	25	326080.39	22	27	134808.83	27	28	269617.66	22	28	−297849.03
25	28	326080.39	27	32	172240.35	24	26	269617.66	21	25	−326080.39
28	29	344480.70				21	23	325089.95	24	27	−269617.66
3	4	357360.98				26	28	372712.06	26	30	−344480.70
3	5	357360.98				27	30	344480.70	27	33	−344480.70
29	33	344480.70				29	31	344480.70	28	31	−344480.70
30	33	344480.70				32	33	344480.70	32	29	−344480.70

the standard one, demonstrating the superiority of clustered tensegrity structures in vibration control due to continuous sliding clustered cables.

Apparently, the FMPC method has good performance in vibration control of tensegrity cantilever beams, and the control effect varies with different control policies, as the number and placement of actuators for each policy are distinctive. Figure 5 exhibits the comparative results on control effect of observed node 33 with different control policies. Interestingly, some significant information can be addressed by taking a deep look at Table 5:

(1) For a standard or clustered tensegrity beam with identical placement of actuators, better control rates can be acquired with the increasing number of actuators. For example, readers can refer to the results of control policies with actuators placed on nodes (6, 11, 16) or (6, 11, 16, 21) for standard tensegrity beam, or control policies with actuators placed on nodes (17, 22, 27) or (17, 22, 27, 32) for clustered tensegrity beam.

(2) For a standard or clustered tensegrity beam with identical number of actuators, the closer the

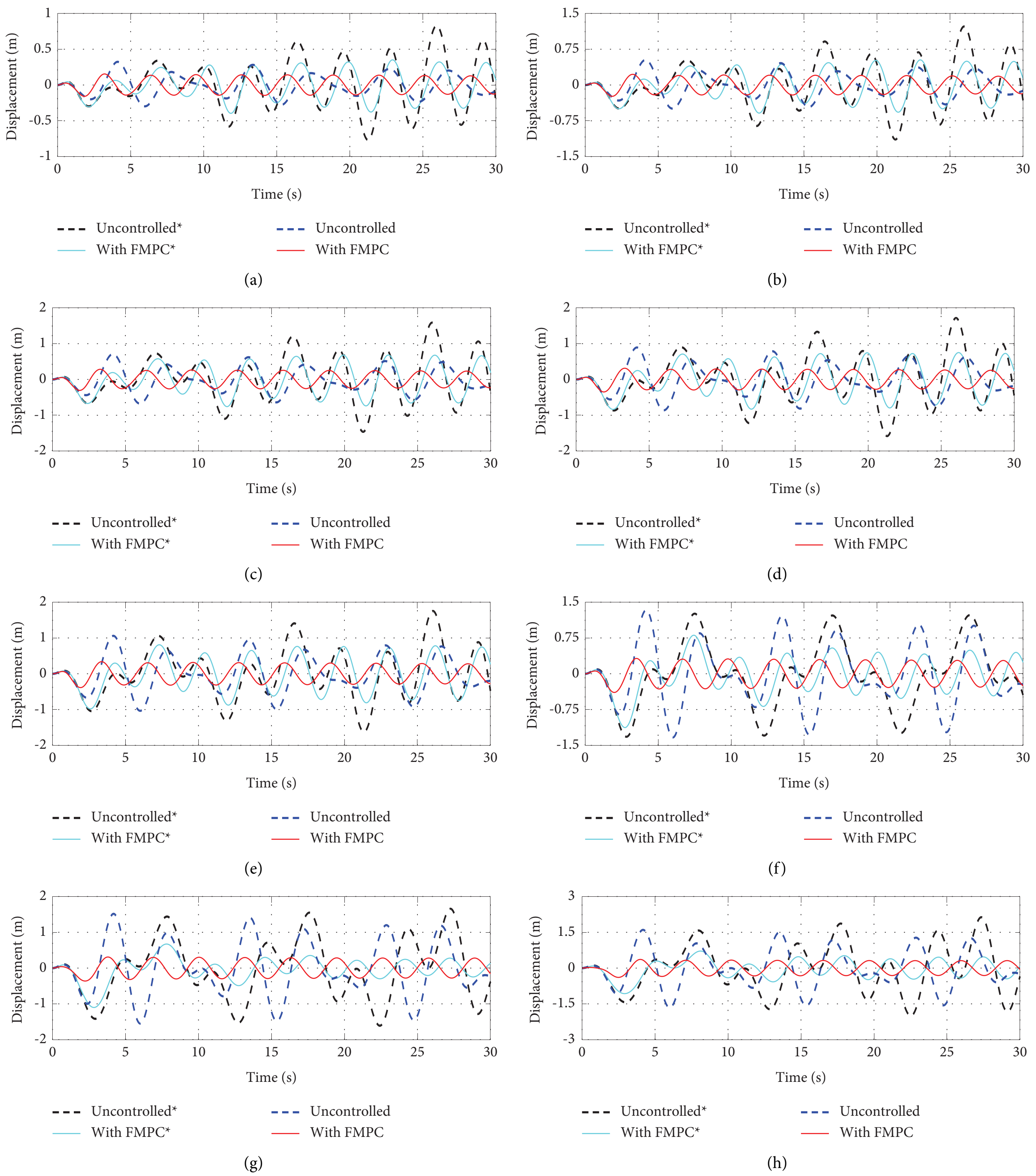

FIGURE 4: Nodal displacement responses for standard and clustered tensegrity beams in the Z-direction: (a) node 10, (b) node 12, (c) node 15, (d) node 17, (e) node 20, (f) node 25, (g) node 30, and (h) node 32.

actuators are placed to the observation point, the better the control rate can be achieved. For example, readers can refer to the results of control policies with three actuators placed on nodes (11, 12, 13) or (21, 22, 23) for standard tensegrity beam, or control policies with four actuators placed on nodes (13, 14, 15, 18) or (23, 24, 25, 28) for clustered tensegrity beam.

(3) For a standard or clustered tensegrity beam with same control condition, namely, identical number of actuators and distance to the observation point, the control rates are nearly the same for actuators placed

Table 4: The comparative results on maximum displacement and the control efficiency of two tensegrities.

Node number	Standard tensegrity beam			Clustered tensegrity beam		
	Uncontrolled (m)	With FMPC (m)	Control rate (%)	Uncontrolled (m)	With FMPC (m)	Control rate (%)
10	0.83	0.35	57.54	0.32	0.09	72.31
12	1.23	0.53	57.05	0.53	0.15	72.09
15	1.59	0.68	56.99	0.71	0.20	71.93
17	1.72	0.75	56.26	0.89	0.25	71.53
20	1.75	0.81	53.84	1.06	0.31	71.19
25	1.26	0.81	35.86	1.33	0.39	70.66
30	1.66	0.67	59.46	1.52	0.44	70.71
32	2.13	0.71	66.50	1.60	0.47	70.83

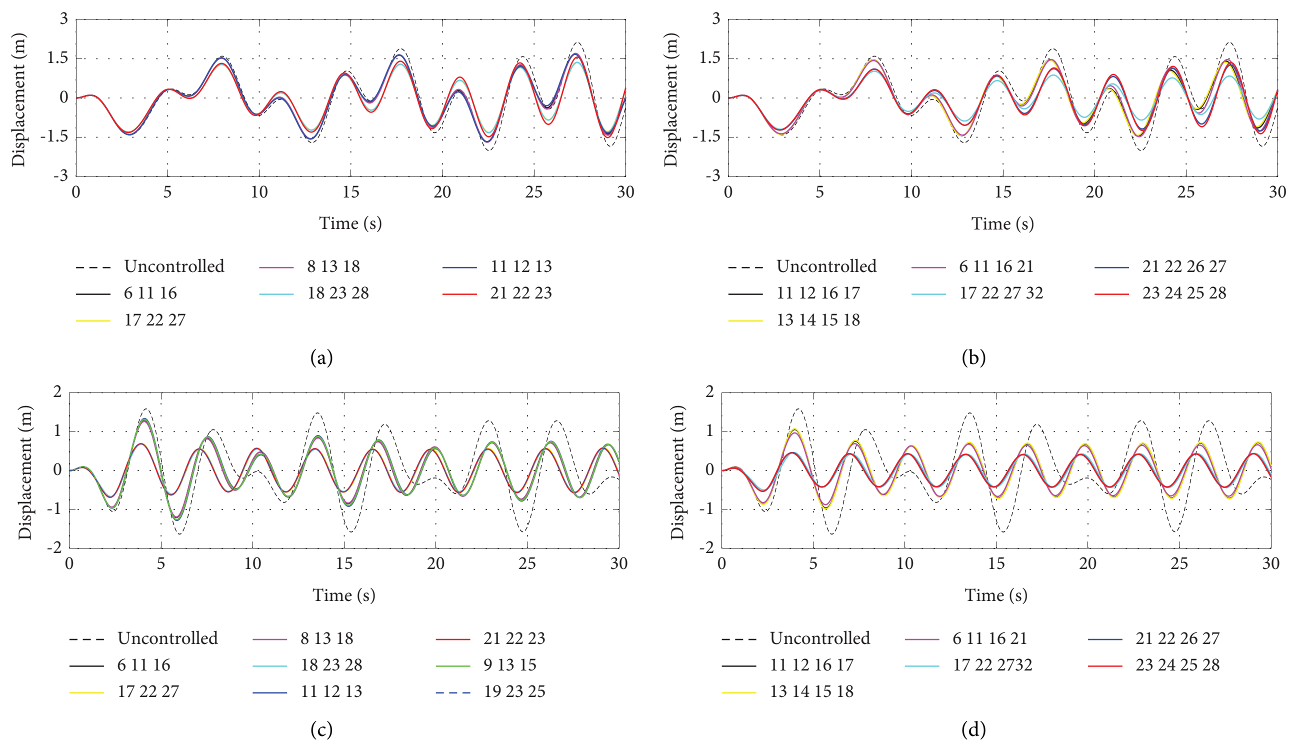

Figure 5: Displacement curves of node 33 in Z- direction for standard and clustered tensegrity beams with different control policies: (a) standard tensegrity beam with three actuators, (b) standard tensegrity beam with four actuators, (c) clustered tensegrity beam with three actuators, and (d) clustered tensegrity beam with four actuators.

on upper or lower nodes. For example, readers can refer to the results of control policies with three actuators placed on nodes (6, 11, 16) or (8, 13, 18) for standard tensegrity beam, or control policies with four actuators placed on nodes (21, 22, 26, 27) or (23, 24, 25, 28) for clustered tensegrity beam.

(4) For most cases, the control rates of the clustered tensegrity beam are significantly higher than those of the standard tensegrity beam with identical control policy, confirming the superiority of clustered tensegrity structures in vibration control.

5.2. A Six-Layer Clustered Tensegrity Tower. A six-layer clustered tensegrity tower (Figure 6), which consists of six quadruple units with 24 struts and 60 cables, is herein utilized to search for optimal control policy. Similarly, 24 clustered cables are denoted by dashed lines in four colors, and line in the same color represents a clustered cable with identical attribute. The solid lines in purple and grey represent the struts and standard cables, respectively. Nodes 3, 17, 10, and 24 are fully constrained. Table 6 shows the information of structural parameters, and the elemental prestress is given in Table 7. The external loadings, given in (40), are applied in the X-direction on each node with time step of 0.020 s.

$$\mathbf{P}(t) = -10000 \sin(2t + 40), \quad t \in [\,0 \;\; 30\,]. \tag{39}$$

In this example, the aforementioned artificial fish swarm algorithm is carried out to search for optimal control policies with given number of actuators, and the following

Table 5: The comparative results on control effect of node 33 with different control strategies.

The control policies		Displacement of node 33			
Uncontrolled		Standard tensegrity beam 2.13 m		Clustered tensegrity beam 1.59 m	
	Actuation position	Maximum value (m)	Control rate (%)	Maximum value (m)	Control rate (%)
Three actuators	6 11 16	1.68	21.30	—	—
	17 22 27	1.35	36.61	—	—
	8 13 18	1.70	20.10	—	—
	18 23 28	1.36	36.03	—	—
	11 12 13	1.67	21.58	—	—
	21 22 23	1.56	26.76	—	—
	6 11 16	—	—	1.27	19.86
	17 22 27	—	—	0.70	56.22
	8 13 18	—	—	1.26	20.67
	18 23 28	—	—	0.68	57.06
	11 12 13	—	—	1.34	15.96
	21 22 23	—	—	0.69	56.69
Four actuators	11 12 16 17	1.46	31.31	—	—
	13 14 15 18	1.46	31.31	—	—
	6 11 16 21	1.47	31.15	—	—
	17 22 27 32	1.23	42.21	—	—
	21 22 26 27	1.26	40.84	—	—
	23 24 25 28	1.35	36.63	—	—
	11 12 16 17	—	—	1.05	33.67
	13 14 15 18	—	—	1.07	32.53
	6 11 16 21	—	—	0.97	39.13
	17 22 27 32	—	—	0.46	70.82
	21 22 26 27	—	—	0.46	70.90
	23 24 25 28	—	—	0.45	71.45

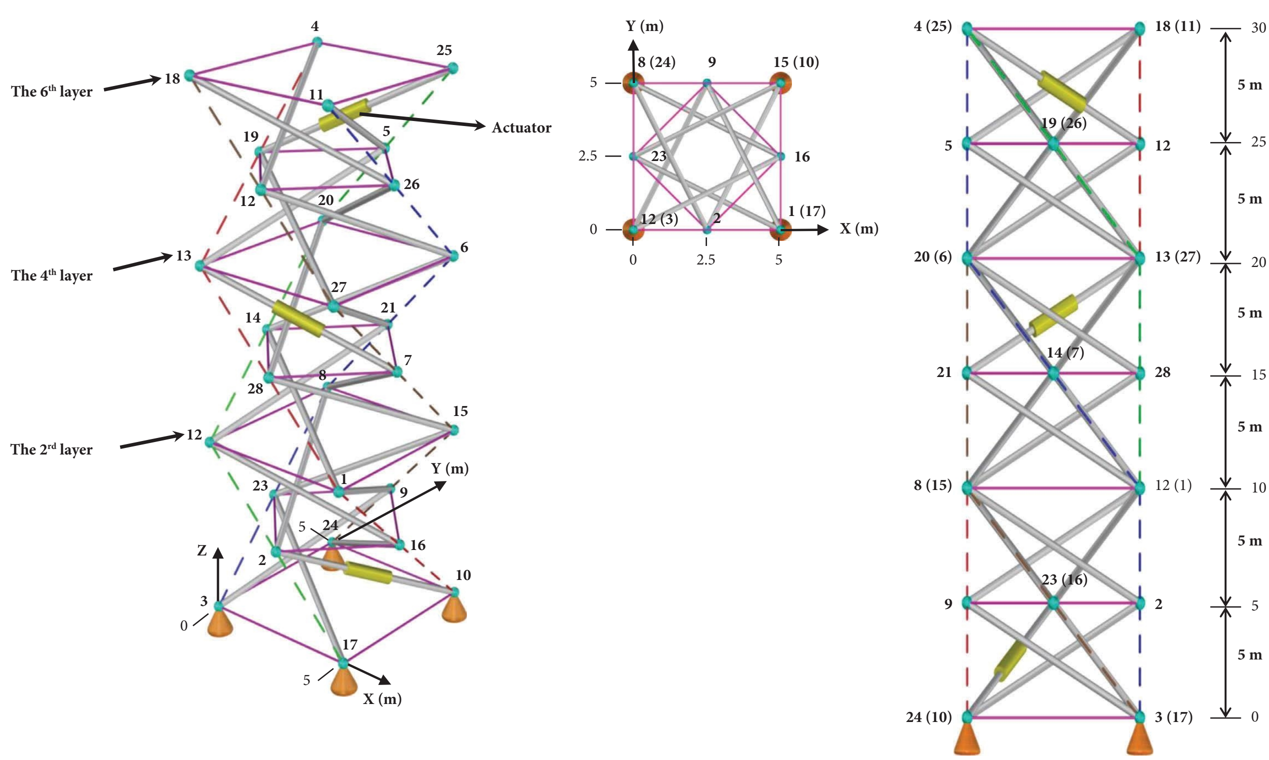

(a) (b) (c)

Figure 6: A six-layer clustered tensegrity tower: (a) perspective view, (b) top view, and (c) side view.

Table 6: Parameters of a six-layer clustered tensegrity tower.

Parameter	Value
Cross section of struts	$3.2 \times 10^{-2} m^2$
Cross section of cables	$1 \times 10^{-3} m^2$
Young's modulus of struts	200×10^9 Pa
Young's modulus of cables	40×10^9 Pa
Density of components	7800 kg/m^3
Prestress in components	Refer to Table 7

Table 7: Prestress for clustered tensegrity tower.

Outer bracing cables			Horizontal cables			Struts		
Node number		Prestress (N)	Node number		Prestress (N)	Node number		Prestress (N)
3	2	219567.41	3	17	109783.71	3	16	−219567.41
1	2	219567.41	17	10	109783.71	17	9	−219567.41
1	7	219567.41	10	24	109783.71	10	23	−219567.41
6	7	219567.41	24	3	109783.71	24	2	−219567.41
6	5	219567.41	4	25	109783.71	4	26	−219567.41
4	5	219567.41	25	11	109783.71	25	12	−219567.41
10	9	219567.41	11	18	109783.71	11	19	−219567.41
8	9	219567.41	18	4	109783.71	18	5	−219567.41
8	14	219567.41	19	12	439134.83	8	16	−219567.41
13	14	219567.41	5	19	439134.83	15	2	−219567.41
13	12	219567.41	26	5	439134.83	1	23	−219567.41
11	12	219567.41	12	26	439134.83	22	9	−219567.41
17	16	219567.41	23	2	439134.83	20	12	−219567.41
15	16	219567.41	9	23	439134.83	6	19	−219567.41
15	21	219567.41	16	9	439134.83	27	5	−219567.41
20	21	219567.41	2	16	439134.83	13	26	−219567.41
20	19	219567.41	21	14	439134.83	20	7	−219567.41
18	19	219567.41	7	21	439134.83	6	28	−219567.41
24	23	219567.41	28	7	439134.83	27	14	−219567.41
22	23	219567.41	14	28	439134.83	13	21	−219567.41
22	28	219567.41	8	15	109783.71	8	28	−219567.41
27	28	219567.41	15	1	109783.71	15	14	−219567.41
27	26	219567.41	1	22	109783.71	1	21	−219567.41
25	26	219567.41	22	8	109783.71	22	7	−219567.41
			20	13	109783.71			
			6	20	109783.71			
			27	6	109783.71			
			13	27	109783.71			
			20	6	109783.71			
			6	27	109783.71			
			27	13	109783.71			
			13	20	109783.71			
			8	22	109783.71			
			15	8	109783.71			
			1	15	109783.71			
			22	1	109783.71			

optimization model is formulated to mitigate structural vibration:

$$\text{minimize } f(x) = \sum_{i=1}^{24}\left(\alpha\left|\overline{U}_{\mathrm{i}}(x)\right| + \beta\left|U_{\mathrm{i}}(x)\right|_{\max}\right),$$
$$\text{subject to}\begin{cases} 0 < \alpha \leq 1, \\ 0 < \beta \leq 1, \\ 1 \leq x \leq 28, x \neq 3, 10, 17, 24, \end{cases} \tag{40}$$

where x is a variable representing the expected placement of actuators, which ranges from 1 to 28 (the tower has 28 nodes with 4 fixed nodes 3, 10, 17, and 24), i is the node number, α and β are the weight coefficients designated by designers, $\overline{U}_{\mathrm{i}}(x)$ is the average amplitude in X-direction of node i within the observation time (30 s), and $|U_{\mathrm{i}}|_{\max}$ is the maximum amplitude in X-direction of node i within the observation time (30 s).

In the case of control policy with four actuators, the parameters in the AFSA algorithm are set as follows: N = 180 (number of artificial fish), MaxGen = 150 (maximum

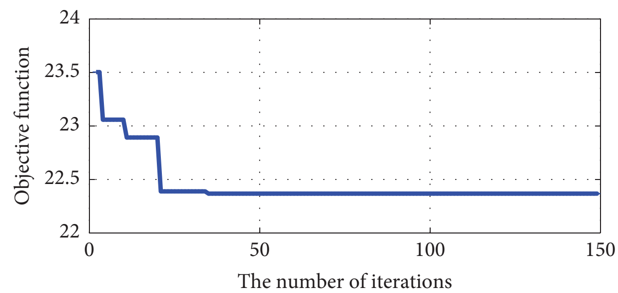

Figure 7: The convergence process of the proposed algorithm in computing the objective function.

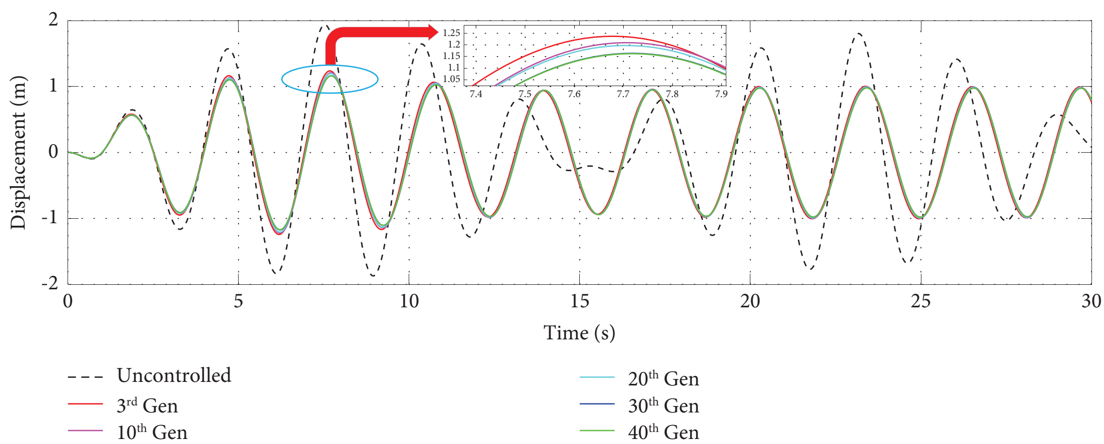

Figure 8: The displacement curves of node 25 in X-direction for the 3rd, 10th, 20th, 30th, and 40th iteration, respectively.

Table 8: The maximum displacements and the corresponding control rates for each layer.

Height (m)	Node number	Max. displacement (m) Uncontrolled	With FMPC	Control rate (%)
5	9	0.12	0.07	41.67
10	15	0.45	0.26	42.22
15	28	0.84	0.48	42.86
20	13	1.24	0.72	41.94
25	12	1.61	0.93	42.24
30	18	1.94	1.13	41.75

number of iterations), Try_number = 5 (maximum test number of prey), Step = 2 (moving step), Delta = 0.423 (congestion factor), and Visual = 1.0 (perception of distance). Figure 7 displays the ladder-like convergent curve of the objective function, in which four stages are shown clearly during the optimization process. The results imply that the feasible actuator positions are obtained at the 3rd, 10th, 20th, and 30th generations, with actuators placed on nodes (6, 11, 12, 18), (4, 5, 18, 19), (4, 6, 11,18), and (4, 11, 18, 19), respectively. The optimal solution is acquired at the 40th generation with the placement of actuators on nodes (4, 11, 12, 18). Nevertheless, if we take a deep look at Figure 8, it can be found that the feasible solutions derived at the 3rd, 10th, 20th, and 30th generations are quite close to the optimal one attained at the 40th generation in mitigating the vibration of the clustered tower as node 25 has the maximum displacement in X-direction under external loadings, proving the fast searching ability in optimization using FMPC and AFSA. More importantly, Table 8 depicts the results of maximum displacement for each tower layer with and without control. Apparently, the maximum displacement of the tensegrity tower emerges at the upper layer with an effective control rate of 41.75% under the obtained optimal control policy, indicating the validity of the presented algorithm in active vibration control of clustered tensegrity structures. Additionally, according to the aforementioned optimal actuator placement, Figure 9 gives the displacement-force curvature of actuators with regard to the observation nodes on the 2nd, 4th, and 6th layer, respectively. It can be concluded that for each actuator under the same observation node, the actuator force is relatively uniform and the amplitude will not exceed the saturation value preset on the actuator, which confirms the validity of the proposed control strategy in guaranteeing the stability of actuator performance during work.

To further investigate the factors that may influence the searching quality in the optimization procedure, two crucial indictors are herein considered, namely, the number of iterations/generations and artificial fish. A total of twelve cases are fully discussed, i.e., Case I (30 fish with 30 generations), Case II (30 fish with 60 generations), Case III (30 fish with 90 generations), Case IV (30 fish with 120 generations), Case V (30 fish with 150 generations), Case

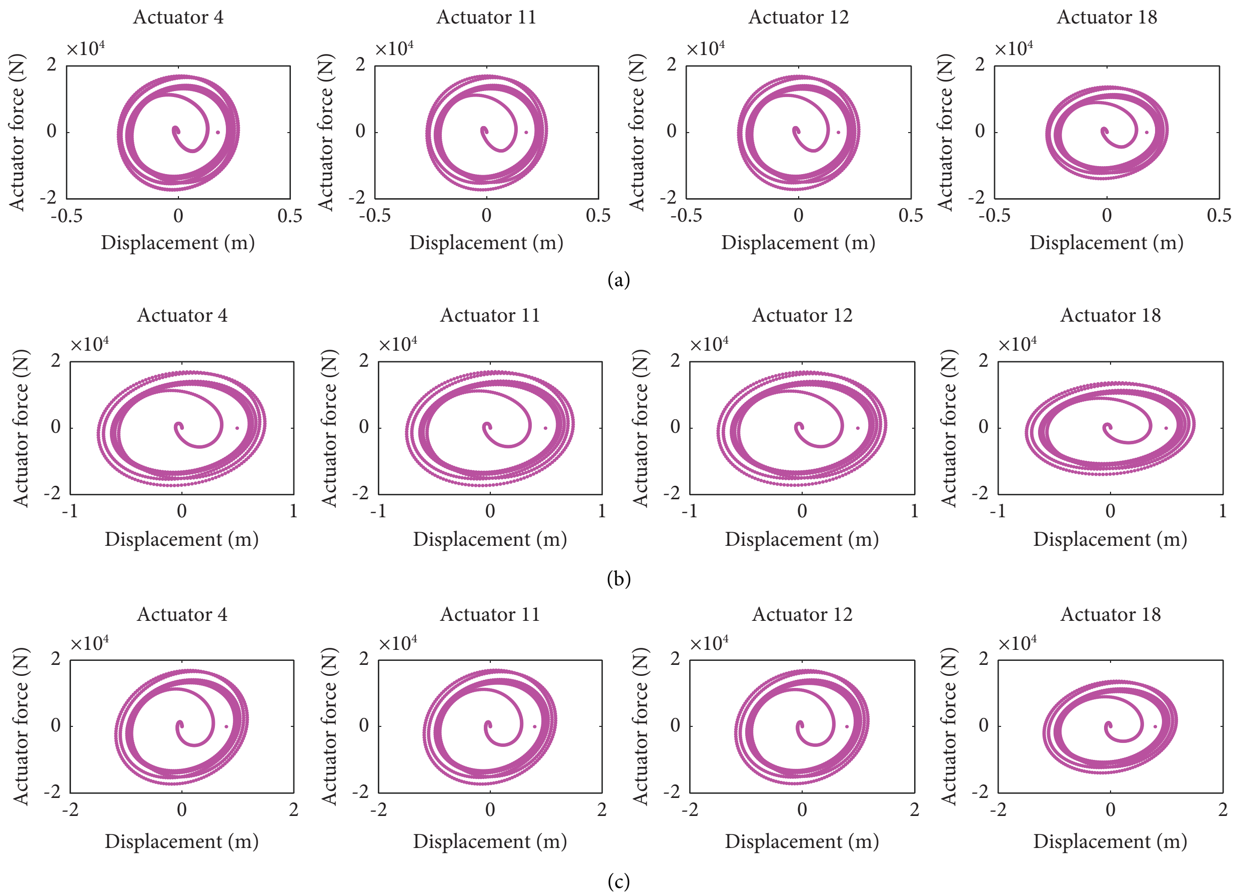

FIGURE 9: The relationship between the nodal displacement in X-direction and the actuator forces on the obtained optimal position of actuators: (a) node 15 on the 2nd layer; (b) node 13 on the 4th layer; (c) node 18 on the 6th layer.

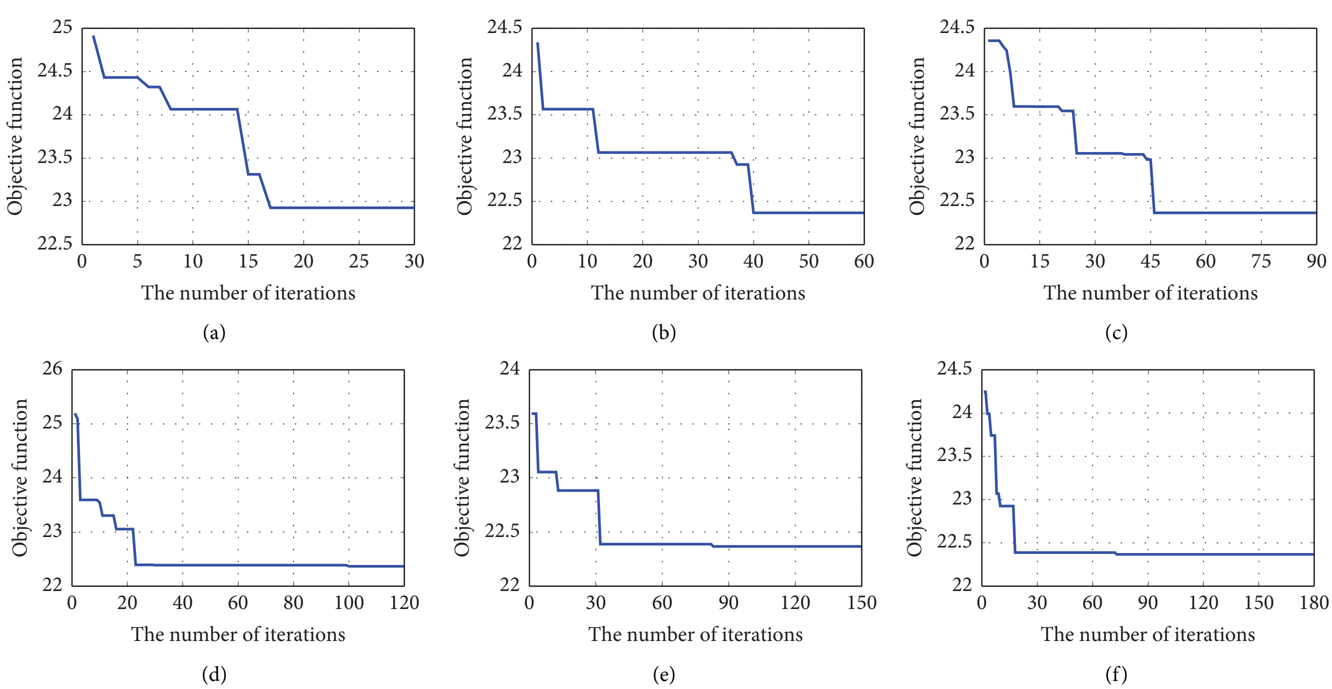

FIGURE 10: Optimization process of the objective function with 30 artificial fish under different number of iterations: (a) 30 generations; (b) 60 generations; (c) 90 generations; (d) 120 generations; (e) 150 generations; (f) 180 generations.

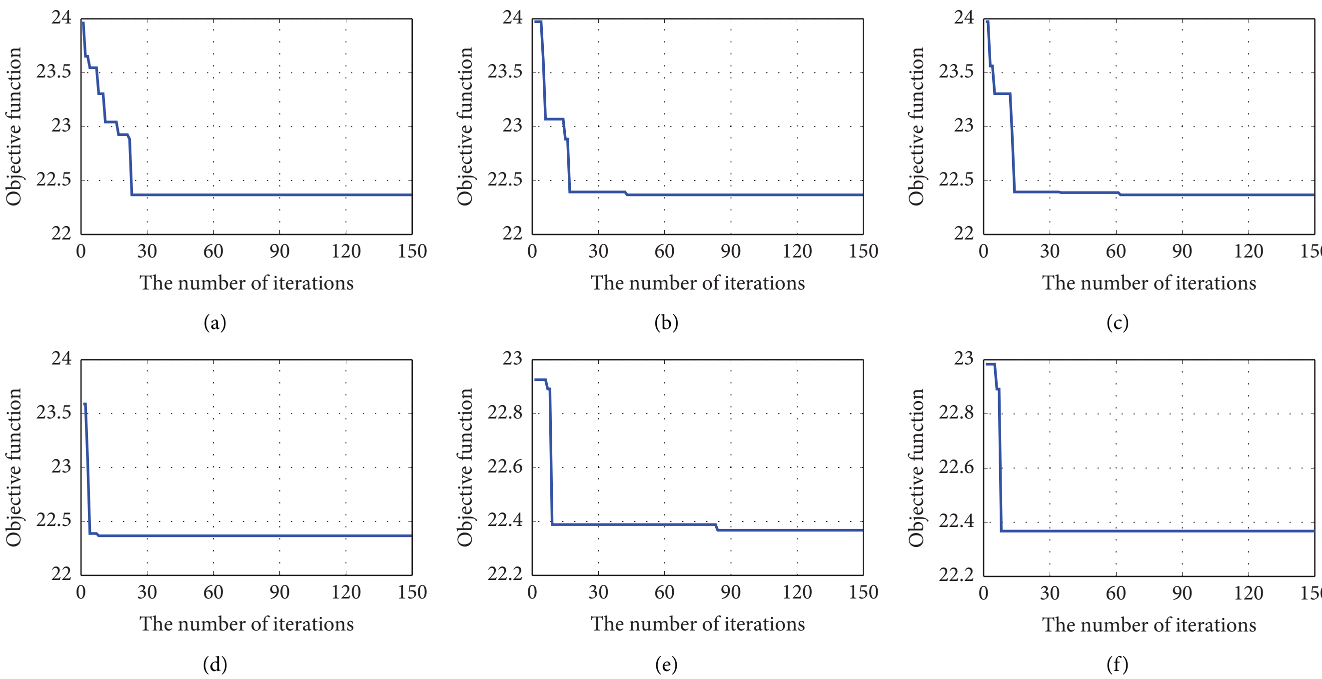

Figure 11: Optimization process of the objective function with different fish number under 150 generations: (a) 60 artificial fish; (b) 80 artificial fish; (c) 100 artificial fish; (d) 120 artificial fish; (e) 140 artificial fish; (f) 160 artificial fish.

Table 9: The process optimization data for twelve cases.

Iterations	5	10	15	20	25	30	35	40	45	50
Casa I	0.8062	0.9173	1.5103	1.6139	1.6139	1.6139	—	—	—	—
Casa II	0.0619	0.7600	0.7616	0.7616	1.3016	1.3016	1.3016	1.3135	1.3730	1.9891
Casa III	0.0619	0.7600	0.7616	0.7616	1.3016	1.3016	1.3016	1.3135	1.3730	1.9891
Casa IV	0.0619	0.7600	0.7616	0.7616	1.3016	1.3016	1.3016	1.3135	1.3730	1.9891
Casa V	0.0619	0.7600	0.7616	0.7616	1.3016	1.3016	1.3016	1.3135	1.3730	1.9891
Casa VI	0.0619	0.7600	0.7616	0.7616	1.3016	1.3016	1.3016	1.3135	1.3730	1.9891
Casa VII	0.4515	0.4515	0.4515	1.0535	1.6428	1.6696	1.6696	1.6696	1.6696	1.6696
Casa VIII	1.5460	1.5895	2.3067	2.8099	2.8099	2.8309	2.8309	2.8309	2.8309	2.8309
Casa IX	0.4804	0.4804	0.6610	1.1777	1.1777	1.1777	1.1777	1.1777	1.1777	1.1777
Casa X	0.0000	0.1740	0.6906	0.6906	0.6906	0.6906	0.6906	0.6906	0.6906	0.6906
Casa XI	0.7350	1.9302	1.9302	1.9302	1.9302	1.9302	1.9302	1.9302	1.9302	1.9302
Casa XII	0.7676	1.2843	1.2843	1.2843	1.2843	1.2843	1.2843	1.2843	1.2843	1.2843

VI (30 fish with 180 generations), Case VII (60 fish with 150 generations), Case VIII (80 fish with 150 generations), Case IX (100 fish with 150 generations), Case X (120 fish with 150 generations), Case XI (140 fish with 150 generations), and Case XII (160 fish with 150 generations). Figure 10 gives the convergence curves of different generations in the optimization process of the objective function with 30 artificial fish. The value of the objective function reaches 22.9259, 22.3675, 22.3675, 22.3675, 22.3675, and 22.3675 for generation of 30, 60, 90, 120, 150, and 180, respectively, implying that reasonable selection of generation is critical as small iterations will lead to divergence of the optimization problem. Another index is the fish number, as is shown in Figures 11(a)–11(c), multiple platforms are emerged during the optimization process of the objective function. However, as is displayed in Figures 11(d)–11(f), these platforms diminish with the raising of the fish number. Moreover, the searching speed is also accelerated with the configuration of more artificial fish, and this can be explained by the fact that the probability in finding excellent individuals (the optimal actuator positions) is consequentially improved with increasing number of artificial fish.

Table 9 gives the detailed information regarding the convergence and the iterations for twelve cases. Each item in this table represents the difference between the values of objective function corresponding to the current iteration and the first iteration. As can be seen, under the condition of same fish number, designers can obtain better value of objective function with fewer iterations to save computational time. Moreover, the results from Table 10 imply that with the same condition of total iteration number, designers can accelerate the optimization speed of the algorithm by selecting a reasonable total fish number (30 or 180 in this illustrative example).

Table 10: The input and output information of performing the AFSA algorithm.

Number of fish	Total iteration number	Convergence iteration number	Convergence computing time (min)	Total computing time (min)	Value of objective function
30	30	16	37	70	23.5489
30	60	46	105	137	22.3675
30	90	46	99	194	22.3675
30	120	46	99	258	22.3675
30	150	46	93	303	22.3675
30	180	46	90	351	22.3675
60	150	28	133	712	22.3675
80	150	30	184	922	22.3675
100	150	17	128	1131	22.3675
120	150	14	122	1311	22.3675
140	150	10	99	1485	22.3675
160	150	7	79	1686	22.3675

Table 11: The optimal results of different control policies.

Number of actuators	Optimal placement of actuators	Node number	Displacement (m)	Control rate (%)
0	—	15	0.45	—
		13	1.24	—
		18	1.94	—
3	4 11 18	15	0.29	35.52
		13	0.80	35.45
		18	1.26	35.36
4	4 11 12 18	15	0.27	40.12
		13	0.74	40.02
		18	1.17	39.89
5	4 5 11 12 18	15	0.25	43.80
		13	0.69	43.85
		18	1.09	43.66
6	4 11 12 13 18 19	15	0.24	45.82
		13	0.67	45.91
		18	1.05	45.70
7	4 5 6 11 12 18 19	15	0.23	48.82
		13	0.63	48.88
		18	1.00	48.63

Finally, the optimal control policies concerning various actuators for the 2^{nd} (node 15), 4^{th} (node 13), and 6^{th} (node 18) layers are investigated in detail with the setting of 50 artificial fish and 100 generations (Table 11). It is obvious that the number of actuators plays a positive effect on the enhancement of control efficiency; nevertheless, with the increase of the actuator number, the lifting effect of control rate becomes slower. Moreover, the control rates are close to each other for different layers with identical optimal control policy found by the proposed algorithm, and the structural vibration is successfully mitigated compared to uncontrolled case, demonstrating the validity of the presented method.

6. Conclusions

As a kind of flexible space structure, tensegrity structure is easy to cause structural deformation under external load, so it needs to be controlled efficiently and safely. Among them, cluster tensegrity as a relatively new flexible space structure is also very much needed. In this paper, a novel fast model predictive control method is proposed for standard tensegrity mechanisms and cluster tensegrity structures, and the artificial fish swarm intelligence algorithm is optimized for actuator placement. The results show the following. (1) Fast model predictive control is suitable for standard tensegrity structure and cluster tensegrity structure and has good control effect. (2) The application of artificial fish swarm algorithm in the optimization of actuator layout has obvious effect and achieves the global optimization objective. (3) The study of examples proves the prospect of control method and artificial fish swarm algorithm in solving practical engineering problems.

Therefore, the results of the study are worthy of further research, such as the development of a more efficient control algorithm or a theoretical basis more in line with practical engineering (e.g., time lag problems). In the actuator arrangement optimization, a multi-objective function is set to achieve a more economical and efficient actuator arrangement. This is the next stage to be worked on.

Appendix

$$\begin{cases} \Theta_{11} = b_4 \hat{\mathbf{K}}^{-1} \mathbf{M} + b_1 \hat{\mathbf{K}}^{-1} \mathbf{C}, \\ \Theta_{12} = -\left(b_5 \hat{\mathbf{K}}^{-1} \mathbf{M} + b_2 \hat{\mathbf{K}}^{-1} \mathbf{C} \right), \\ \Theta_{13} = -\left(b_6 \hat{\mathbf{K}}^{-1} \mathbf{M} + b_3 \hat{\mathbf{K}}^{-1} \mathbf{C} \right), \end{cases}$$
$$\begin{cases} \Theta_{21} = b_1 b_4 \hat{\mathbf{K}}^{-1} \mathbf{M} + b_1 b_1 \hat{\mathbf{K}}^{-1} \mathbf{C} - b_1 \mathbf{I}_1, \\ \Theta_{22} = -\left(b_1 b_5 \hat{\mathbf{K}}^{-1} \mathbf{M} + b_1 b_2 \hat{\mathbf{K}}^{-1} \mathbf{C} - b_2 \mathbf{I}_1 \right) \\ \Theta_{23} = -\left(b_1 b_6 \hat{\mathbf{K}}^{-1} \mathbf{M} + b_1 b_3 \hat{\mathbf{K}}^{-1} \mathbf{C} - b_3 \mathbf{I}_1 \right), \end{cases}$$
$$\begin{cases} \Theta_{31} = b_4 b_4 \hat{\mathbf{K}}^{-1} \mathbf{M} + b_1 b_4 \hat{\mathbf{K}}^{-1} \mathbf{C} - b_4 \mathbf{I}_1, \\ \Theta_{32} = -\left(b_4 b_5 \hat{\mathbf{K}}^{-1} \mathbf{M} + b_2 b_4 \hat{\mathbf{K}}^{-1} \mathbf{C} - b_5 \mathbf{I}_1 \right), \\ \Theta_{33} = -\left(b_4 b_6 \hat{\mathbf{K}}^{-1} \mathbf{M} + b_3 b_4 \hat{\mathbf{K}}^{-1} \mathbf{C} - b_6 \mathbf{I}_1 \right), \end{cases} \tag{A.1}$$

$$b_1 = \frac{\delta}{\alpha \Delta t},$$

$$b_2 = 1 - \frac{\delta}{\alpha},$$

$$b_3 = \left(1 - \frac{\delta}{2\alpha} \right) \Delta t,$$

$$b_4 = \frac{1}{\alpha (\Delta t)^2},$$

$$b_5 = \frac{-1}{\alpha \Delta t},$$

$$b_6 = 1 - \frac{1}{2\alpha}.$$

Data Availability

The data used to support the findings of this study are included within the article.

Conflicts of Interest

The authors declare that they have no conflicts of interest.

Acknowledgments

This study was supported by the National Natural Science Foundation of China (grant no. 51908356) and the project from China Scholarship Council (grant no. 202008330250).

References

[1] B. F. Richard, "Tensile-integrity Structures.3063521A," 1962, https://www.freepatentsonline.com/3063521.html.

[2] R. Skelton, R. Montuori, V. Pecoraro, R. Montuori, and V. Pecoraro, "Globally stable minimal mass compressive tensegrity structures," *Composite Structures*, vol. 141, pp. 346–354, 2016.

[3] R. Skelton, R. Adhikari, J. Pinaud, W. Chan, and J. Helton, "An introduction to the mechanics of tensegrity," *IEEE Conference on Decision & Control*, vol. 5, pp. 4254–4259, 2001.

[4] B. Adam, I. F. Smith, and I. F. C. Smith, "Active tensegrity: Active tensegrity: A control framework for an adaptive civil-engineering structure control framework for an adaptive civil-engineering structure," *Computers & Structures*, vol. 86, no. 23-24, pp. 2215–2223, 2008.

[5] B. Maurin, R. Motro, F. Cevaer, V. Raducanu, F. Cevaer, and V. Raducanu, "Composite profiles and membranes tensegrity panels," *European Journal of Environmental and Civil Engineering*, vol. 13, no. 9, pp. 1061–1072, 2009.

[6] S. Korkmaz, N. B. H. Ali, I F. B. H. Smith, and I. F. C. Smith, "Configuration of control system for damage tolerance of a tensegrity bridge," *Advanced Engineering Informatics*, vol. 26, no. 1, pp. 145–155, 2012.

[7] L. Rhode-Barbarigos, N. B. Hadj Ali, R. Motro, I. F. B. H. Smith, R. Motro, and I. F. C. Smith, "Designing tensegrity modules for pedestrian bridges," *Engineering Structures*, vol. 32, no. 4, pp. 1158–1167, 2010.

[8] E. Babilio, R. Miranda, and F. Fraternali, "On the kinematics and actuation of dynamic sunscreens with tensegrity architecture," *Front. Mater.*, vol. 6, p. 7, 2019.

[9] J. Feron, L. Boucher, V. Denoel, and P. Latteur, "Optimization of footbridges composed of prismatic tensegrity modules," *Journal of Bridge Engineering*, vol. 24, no. 12, 2019.

[10] R. Ma, R. Ma, J. K. Guest, R. L. Ma, and J. K. Guest, "Research on optimum design and construction process of tensegrity tower structures," *Advances in Structural Engineering*, vol. 19, no. 3, pp. 409–419, 2016.

[11] D. E. Ingber, "The architecture of life," *Scientific American*, vol. 278, no. 1, pp. 48–57, 1998.

[12] T. Chen, C. C. Wu, M. J. Tang et al., "Complexity of the Complexity of the Tensegrity Structure for Dynamic Energy and Force Distribution of Cytoskeleton during Cell Spreadingensegrity structure for dynamic energy and force distribution of cytoskeleton during cell spreading," *PLoS One*, vol. 5, no. 12, Article ID e14392, 2010.

[13] J. Zheng, J. J. Birktoft, Y. Chen et al., "From molecular to macroscopic via the rational design of a self-assembled 3D DNA crystal," *Nature*, vol. 461, no. 7260, pp. 74–77, 2009.

[14] W. Ning, "Mechanotransduction across the cell surface and through the cytoskeleton," *Trends in Cell Biology*, vol. 3, no. 8, pp. 1124–1127, 1993.

[15] L. Wang, W. L. Chen, and W. Y. Chen, "Modelling Modelling Cell Origami via a Tensegrity Model of the Cytoskeleton in Adherent Cellsell origami via a tensegrity model of the cytoskeleton in adherent cells," *Applied Bionics and Biomechanics*, vol. 2019, Article ID 8541303, 9 pages, 2019.

[16] G. Xu, B. Li, X. Q. Feng et al., "Tensegrity Model of Cell Reorientation on Cyclically Stretched Substratesensegrity model of cell reorientation on cyclically stretched substrates," *Biophysical Journal*, vol. 111, no. 7, pp. 1478–1486, 2016.

[17] A. G. Tibert and S. Pellegrino, "Deployable Tensegrity Deployable Tensegrity Reflectors for Small Satelliteseflectors for

small satellites," *Journal of Spacecraft and Rockets*, vol. 39, no. 5, pp. 701–709, 2002.

[18] S. Yang, C. Sultan, and C. Sultan, "Deployment of foldable tensegrity-membrane systems via transition between tensegrity configurations and tensegrity-membrane configurations," *International Journal of Solids and Structures*, vol. 160, pp. 103–119, 2019.

[19] M. Chen, R. Goyal, M. Majji et al., "Design and analysis of a growable artificial gravity space habitat," *Aerospace Science and Technology*, vol. 106, Article ID 106147, 2020.

[20] J. Zhang, M. Ohsaki, J. J. Rimoli et al., "Optimization for energy absorption of 3-dimensional tensegrity lattice with truncated octahedral units," *Composite Structures*, vol. 267, Article ID 113903, 2021.

[21] C. Sultan, "Tensegrity: 60 Years of art, science, and engineering," *Advances in Applied Mechanics*, vol. 43, pp. 69–145, 2009.

[22] C. Intrigila, A. Micheletti, N A. Nodargi et al., "Fabrication and experimental characterisation of a bistable tensegrity-like unit for lattice metamaterials," *Additive Manufacturing*, vol. 57, Article ID 102946, 2022.

[23] Y. Tian, J. S. Kahn, L. Bai et al., "Ordered three-dimensional nanomaterials using DNA-prescribed and valence-controlled material voxels," *Nature Materials*, vol. 19, no. 7, pp. 789–796, 2020.

[24] J. Bauer, J. A. Kraus, C. Crook, J. J. Rimoli, and L. Valdevit, "T Metamaterials: Toward failure-resistant engineering systems through delocalized deformation," *Advanced Materials*, vol. 33, no. 10, pp. 72–94, 2021.

[25] K. Liu, T. Zegard, P. P. Pratapa, G. H. Paulino, P. P. Pratapa, and G. H. Paulino, "Unraveling tensegrity tessellations for metamaterials with tunable stiffness and bandgaps," *Journal of the Mechanics and Physics of Solids*, vol. 131, pp. 147–166, 2019.

[26] H. Lee, Y. Jang, J. K. Choe et al., "3D-printed programmable tensegrity for soft robotics," *Science Robotics*, vol. 5, no. 45, p. 9024, 2020.

[27] J. Rieffel, J. B. Mouret, and J. B. Mouret, "Adaptive and Adaptive and Resilient Soft Tensegrity Robotsesilient soft tensegrity robots," *Soft Robotics*, vol. 5, no. 3, pp. 318–329, 2018.

[28] C. Paul, F. Valero-Cuevas, H. J. Lipson, and H. Lipson, "Design and control of tensegrity robots for locomotion," *IEEE Transactions on Robotics*, vol. 22, no. 5, pp. 944–957, 2006.

[29] J. Booth, O. Cyr-Choinière, J. C. Case et al., "Surface Surface Actuation and Sensing of a Tensegrity Structure Using Robotic Skinsctuation and sensing of a tensegrity structure using robotic skins," *Soft Robotics*, vol. 8, no. 5, pp. 531–541, 2021.

[30] D. Shah, J. W. Booth, R. L. Baines et al., "Tensegrity Robotics," *Tensegrity Robotics Soft Robot*, vol. 9, no. 4, pp. 639–656, 2022.

[31] A. Tibert and S. Pellegrino, "Review of Review of Form-Finding Methods for Tensegrity Structuresorm-finding methods for tensegrity structures," *International Journal of Space Structures*, vol. 26, no. 3, pp. 241–255, 2011.

[32] S. Juan, J. M. H. Mirats Tur, and J. M. M. Tur, "Tensegrity frameworks: Tensegrity frameworks: Static analysis reviewtatic analysis review," *Mechanism and Machine Theory*, vol. 43, no. 7, pp. 859–881, 2008.

[33] M. Raja, S. G. Narayanan, and S. Narayanan, "Active control of tensegrity structures under random excitation," *Smart Materials and Structures*, vol. 16, no. 3, pp. 809–817, 2007.

[34] B. de Jager, R. D. Skelton, and R. E. Skelton, "Input-output selection for planar tensegrity models," *IEEE Transactions on Control Systems Technology*, vol. 13, no. 5, pp. 778–785, 2005.

[35] A. Wroldsen, M. de Oliveira, R. Skelton, M. C. De Oliveira, and R. E. Skelton, "Modelling and control of non-minimal non-linear realisations of tensegrity systems," *International Journal of Control*, vol. 82, no. 3, pp. 389–407, 2009.

[36] K. Moored, H. W. Bart-Smith, and H. Bart-Smith, "Investigation of clustered actuation in tensegrity structures," *International Journal of Solids and Structures*, vol. 46, no. 17, pp. 3272–3281, 2009.

[37] S. Djouadi, R. Motro, J. Pons, B. Crosnier, J. C. Pons, and B. Crosnier, "Active control of tensegrity systems," *Journal of Aerospace Engineering*, vol. 11, no. 2, pp. 37–44, 1998.

[38] N. Bel Hadj Ali, I. B. H. Smith, and I. F. C. Smith, "Dynamic behavior and vibration control of a tensegrity structure," *International Journal of Solids and Structures*, vol. 47, no. 9, pp. 1285–1296, 2010.

[39] X. Feng, Y. Ou, M. S. Miah, Y. W. Ou, and M. S. Miah, "Energy-based comparative analysis of optimal active control schemes for clustered tensegrity structures," *Structural Control and Health Monitoring*, vol. 25, no. 10, Article ID e2215, 2018.

[40] N. Kanchanasaratool, D. Williamson, and D. Williamson, "Motion control of a tensegrity platform," *Communications in Information and Systems*, vol. 2, no. 3, pp. 299–324, 2002.

[41] S. Amouri, J. Averseng, J. Quirant, J. F. Dube, J. Quirant, and J. F. Dube, "Structural design and control of modular tensegrity structures," *European Journal of Environmental and Civil Engineering*, vol. 19, no. 6, pp. 687–702, 2015.

[42] R. Goyal, M. Majji, R. E. Skelton, and R. E. Skelton, "Integrating structure, information architecture and control design: Integrating structure, information architecture and control design: Application to tensegrity systemspplication to tensegrity systems," *Mechanical Systems and Signal Processing*, vol. 161, Article ID 107913, 2021.

[43] P. Schorr, L. Zentner, K. Zimmermann, V. Böhm, K. Zimmermann, and V. Bohm, "Jumping locomotion system based on a multistable tensegrity structure," *Mechanical Systems and Signal Processing*, vol. 152, Article ID 107384, 2021.

[44] S. Yang, C. Sultan, and C. Sultan, "LPV control of a tensegrity-membrane system," *Mechanical Systems and Signal Processing*, vol. 95, pp. 397–424, 2017.

[45] Y. Tang, T. Li, Q. Lv et al., "A self-vibration-control tensegrity structure for space large-scale construction," *Mechanical Systems and Signal Processing*, vol. 177, Article ID 109241, 2022.

[46] A. Wahrhaftig, K. M. Magalhães, M. Silva et al., "Buckling and free vibration analysis of non-prismatic columns using optimized shape functions and Rayleigh method," *European Journal of Mechanics-A: Solids*, vol. 94, Article ID 104543, 2022.

[47] A. de Macêdo Wahrhaftig, J. G. L. Dantas, R. Fonseca Brasil et al., "Control of the Control of the Vibration of Simply Supported Beams Using Springs with Proportional Stiffness to the Axially Applied Forceibration of simply supported beams using springs with proportional stiffness to the axially applied force," *Journal of Vibration Engineering & Technologies*, vol. 10, no. 6, pp. 2163–2177, 2022.

[48] I. Venanzi, L. Ierimonti, F. Ubertini, and F. Ubertini, "An enhanced nonlinear damping approach accounting for system constraints in active mass dampers," *Journal of Sound and Vibration*, vol. 357, pp. 2–15, 2015.

[49] J. Kim and F. Jabbari, "Scheduled controllers for buildings under seismic excitation with limited actuator capacity," *Journal of Engineering Mechanics*, vol. 130, no. 7, pp. 800–808, 2004.

[50] M. Cychowski, K. Szabat, T. Orlowska-Kowalska, and T. Orlowska-Kowalska, "Constrained Constrained Model Predictive Control of the Drive System With Mechanical Elasticityodel predictive control of the drive system with mechanical elasticity," *IEEE Transactions on Industrial Electronics*, vol. 56, no. 6, pp. 1963–1973, 2009.

[51] Y. Chen, S. Zhang, H. Peng et al., "A novel fast model predictive control for large-scale structures," *Journal of Vibration and Control*, vol. 23, no. 13, pp. 2190–2205, 2017.

[52] H. Peng, F. Li, S. Zhang et al., "A novel fast model predictive control with actuator saturation for large-scale structures," *Computers & Structures*, vol. 187, pp. 35–49, 2017.

[53] G. Takacs, B. Rohal'-Ilkiv, and B. Rohal'-Ilkiv, "Model predictive control algorithms for active vibration control: a study on timing, performance and implementation properties," *Journal of Vibration and Control*, vol. 20, no. 13, pp. 2061–2080, 2014.

[54] G. Mei, A. Kareem, and J. C. Kantor, "Real-time model predictive control of structures under earthquakes," *Earthquake Engineering & Structural Dynamics*, vol. 30, no. 7, pp. 995–1019, 2001.

[55] H. J. Peng, Q. Gao, Z. G. Wu, and W. X. Zhong, "Fast model predictive control method for large-scale structural dynamic systems: computational aspects," *Shock and Vibration*, vol. 2014, Article ID 508954, 13 pages, 2014.

[56] M. Neshat, G. Sepidnam, M. Sargolzaei, A. N. Toosi, M. Sargolzaei, and A. N. Toosi, "Artificial fish swarm algorithm: a survey of the state-of-the-art, hybridization, combinatorial and indicative applications," *Artificial Intelligence Review*, vol. 42, no. 4, pp. 965–997, 2014.

[57] C. Ma, R. X. He, and R. C. He, "Green wave traffic control system optimization based on adaptive genetic-artificial fish swarm algorithm," *Neural Computing and Applications*, vol. 31, no. 7, pp. 2073–2083, 2019.

[58] N. Fang, J. Zhou, R. Zhang et al., "A hybrid of real coded genetic algorithm and artificial fish swarm algorithm for short-term optimal hydrothermal scheduling," *International Journal of Electrical Power & Energy Systems*, vol. 62, pp. 617–629, 2014.

[59] X. Luan, Z. P. Li, T. Z. Liu, Z. P. Li, and T. Z. Liu, "A novel attribute reduction algorithm based on rough set and improved artificial fish swarm algorithm," *Neurocomputing*, vol. 174, pp. 522–529, 2016.

[60] G. Yuan, W. H. Yang, and W. X. Yang, "Study on optimization of economic dispatching of electric power system based on Hybrid Intelligent Algorithms (PSO and AFSA)," *Energy*, vol. 183, pp. 926–935, 2019.

[61] L. Zhang, M. Lu, H. Zhang, B. Yan, H. Zhang, and B. Yan, "Geometrically nonlinear elasto-plastic analysis of clustered tensegrity based on the co-rotational approach," *International Journal of Mechanical Sciences*, vol. 93, pp. 154–165, 2015.

[62] L. Li, Z. Shao, and J. Qian, "An optimizing method based on autonomous animate: fish swarm algorithm," *Syst. Eng. Theory Pract.*, vol. 22, pp. 32–38, 2002.

[63] X. D. Feng, W. P. Zhang, Y. Z. Luo, and S. Zlotnik, "Optimal prestress investigation on tensegrity structures using artificial fish swarm algorithm," *Advances in Civil Engineering*, vol. 2020, Article ID 1942373, 10 pages, 2020.

[64] X. Feng, S. D. Guo, and S. H. Guo, "Geometrical nonlinear elasto-plastic analysis of tensegrity systems via the co-rotational method," *Mechanics Research Communications*, vol. 79, pp. 32–42, 2017.

[65] X. Feng, S. D. Guo, and S. H. Guo, "A novel method of determining the sole configuration of tensegrity structures," *Mechanics Research Communications*, vol. 69, pp. 66–78, 2015.

[66] X. D. Feng, "The optimal initial self-stress design for tensegrity grid structures," *Computers & Structures*, vol. 193, pp. 21–30, 2017.